Article

Neuron

Control of Mitral/Tufted Cell Output by Selective Inhibition among Olfactory Bulb Glomeruli

Highlights

- Odor-evoked mitral cell excitation and suppression map to interspersed glomeruli
- Within a glomerulus, response polarity is shared across mitral cells
- Interglomerular inhibition can potently suppress excitatory odorant responses
- Functional inhibition among glomerular ensembles is sparse and odorant specific

Authors

Michael N. Economo, Kyle R. Hansen, Matt Wachowiak

Correspondence

matt.wachowiak@utah.edu

In Brief

Economo et al. show that odorants evoke combinatorial patterns of mitral cell excitation and suppression that map to discrete olfactory bulb glomeruli and find evidence that interglomerular inhibitory circuits selectively and nonrandomly regulate mitral cell output among odorant-specific glomerular ensembles.

Economo et al., 2016, Neuron *91*, 1–15
July 20, 2016
http://dx.doi.org/10.1016/j.neuron.2016.06.001

CellPress

Please cite this article in press as: Economo et al., Control of Mitral/Tufted Cell Output by Selective Inhibition among Olfactory Bulb Glomeruli, Neuron (2016), http://dx.doi.org/10.1016/j.neuron.2016.06.001

Neuron
Article

Control of Mitral/Tufted Cell Output by Selective Inhibition among Olfactory Bulb Glomeruli

Michael N. Economo,[1] Kyle R. Hansen,[1] and Matt Wachowiak[1,*]
[1]Brain Institute and Department of Neurobiology and Anatomy, University of Utah, Salt Lake City, UT 84112, USA
*Correspondence: matt.wachowiak@utah.edu
http://dx.doi.org/10.1016/j.neuron.2016.06.001

SUMMARY

Inhibition is fundamental to information processing by neural circuits. In the olfactory bulb (OB), glomeruli are the functional units for odor information coding, but inhibition among glomeruli is poorly characterized. We used two-photon calcium imaging in anesthetized and awake mice to visualize both odorant-evoked excitation and suppression in OB output neurons (mitral and tufted, MT cells). MT cell response polarity mapped uniformly to discrete OB glomeruli, allowing us to analyze how inhibition shapes OB output relative to the glomerular map. Odorants elicited unique patterns of suppression in only a subset of glomeruli in which such suppression could be detected, and excited and suppressed glomeruli were spatially intermingled. Binary mixture experiments revealed that interglomerular inhibition could suppress excitatory mitral cell responses to odorants. These results reveal that inhibitory OB circuits nonlinearly transform odor representations and support a model of selective and nonrandom inhibition among glomerular ensembles.

INTRODUCTION

Synaptic inhibition is fundamental to information processing by cortical networks. In sensory systems including vision, somatosensation, and audition, inhibitory circuits impact response features such as the gain, threshold, and selectivity of responses to sensory stimuli (Isaacson and Scanziani, 2011). However, for olfaction—a primary sensory modality for most mammals—little is known about how inhibitory processing shapes odorant responses or how inhibitory circuits are engaged by natural odorant sampling. In the olfactory bulb (OB), the first stage of olfactory processing, multiple inhibitory circuits impact OB output via mitral/tufted (MT) cells (Fukunaga et al., 2014; Shao et al., 2009; Wachowiak and Shipley, 2006). Characterizing these circuits in vitro has led to hypotheses for how inhibition shapes odor coding that include sharpening or decorrelation of odor representations, gain control, filtering weak inputs, temporally shaping MT spike patterns, and synchronizing MT spike timing (Cleland and Linster, 2012; Gire and Schoppa, 2009; Najac et al., 2015; Shao et al., 2013). With few exceptions, however (Banerjee et al., 2015; Fukunaga et al., 2014; Kato et al., 2013; Yokoi et al., 1995), these hypotheses remain largely untested in vivo.

In the early olfactory system, the functional unit of coding is the glomerulus, which represents sensory input from a single odorant receptor and is the singular site of excitatory input onto MT cells projecting to olfactory cortex. MT cell responses to sensory input are shaped by both intraglomerular inhibitory circuits (i.e., feedforward or recurrent inhibition in the glomerular neuropil) and interglomerular circuits (i.e., lateral inhibition). Intra- and interglomerular circuits appear to have distinct and dissociable roles in shaping MT odor responses (Aungst et al., 2003; Fukunaga et al., 2014; Shao et al., 2012, 2013). However, to fully test predictions for how OB inhibitory circuits impact odor representations, it is critical to relate functional measures of inhibition to odor space and to the glomeruli that represent the functional modules of odor coding at this stage.

In the present study, we used in vivo two-photon GCaMP imaging to visualize sensory-driven inhibition in the OB of awake and anesthetized mice, as reflected in the suppression of activity imaged from MT somata and their apical dendritic tufts. This approach allowed us to characterize how inhibition shapes odor representations at the level of MT output and in the context of the OB glomerular map. We found that odorant-evoked inhibition potently suppresses output from MT cells innervating the same glomerulus and that this suppression is selective for particular glomeruli and odorant specific. A given odorant excites and suppresses a specific combination of spatially intermingled glomeruli, and MT output from a glomerulus is excited or suppressed by a distinct combination of odorants. Using odorant mixtures, we showed that this suppression is sufficiently strong to gate excitatory responses to other odorants. We further found that odorant-specific MT cell suppression is mediated, at least in part, by interglomerular inhibitory interactions that appear to nonrandomly target glomeruli across the dorsal OB and differentially target deep versus superficial MT cells. These results reveal a previously unseen level of specificity in the impact of inhibitory circuits on OB output patterns and a surprising richness in the representation of odors at the level of glomerular maps.

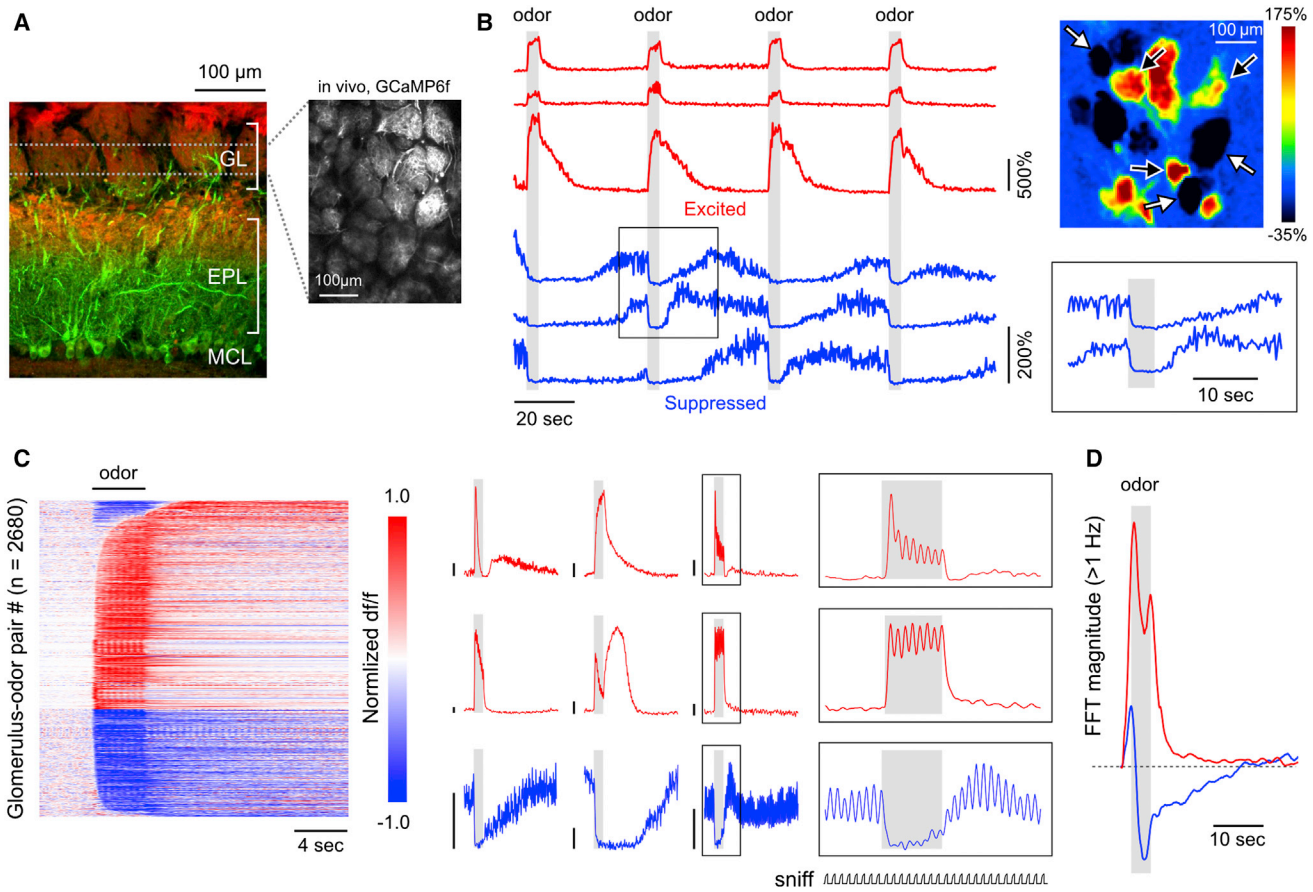

Figure 1. Odorant-Evoked Excitation and Suppression Map to Discrete OB Glomeruli in Anesthetized Mice

(A) Left: reference image showing retrograde GCaMP expression in piriform cortex-projecting mitral and tufted (pcMT) cells, in this case expressed in a PCdh21-Cre:Rosa26-tdTomato mouse (to better visualize OB lamina). GCaMP expression was restricted to cells with somata in the mitral cell layer (MCL) and lateral dendrites in the deep ~2/3 of the external plexiform layer (EPL; green). Red label shows tdTomato expression in olfactory sensory neurons in the glomerular layer (GL) as well as in mitral and tufted cells. Right: two-photon image of GCaMP expression in the dorsal OB in vivo (right).

(B) Time series (left) and spatial map (top right) of odorant-evoked fluorescence changes evoked by four presentations of the same odorant. Excited (black arrows, red traces) and suppressed (white arrows, blue traces) glomeruli are intermingled. Traces from suppressed glomeruli show that, during epochs of elevated spontaneous activity, odorants elicit an abrupt decrease in both the intensity and variability of fluorescence (expanded in inset, bottom right), which slowly recovers after odorant offset.

(C) Left: odorant-evoked GCaMP signals across a population of glomerulus-odor pairs sorted by latency separately for excited (top) and suppressed (bottom) cells. Each row represents one glomerulus-odor pair, with time along the horizontal axis. Responses were normalized by their maximum or minimum value for excitatory and suppressive responses respectively. In this plot, responses were categorized as excitatory if there was only a significant excitatory response or both excitatory and suppressive responses. Middle: example time series from nine glomerulus-odor pairs illustrate the diversity of temporal response patterns. Each trace is the average of eight trials, with the timing of artificial inhalation and odorant presentation synchronized across trials. Scale bars represent 25% ΔF/F. Right: expanded view of boxed regions from three glomerulus-odor pairs illustrates inhalation-linked excitatory modulation (top two traces) and suppression of inhalation-linked activity by the odorant (bottom trace). Inhalation coupling is evident in anesthetized, tracheotomized mice in this artificial inhalation paradigm. Lower trace ("sniff") indicates sequence of inhalations.

(D) Time course of the summed FFT amplitude in the >1 Hz band across all glomerulus-odor pairs displaying excitatory (red) and suppressive responses (blue). Each point represents amplitude in a 4 s window centered at the time indicated. Note that the initial downward deflection of the fluorescence time series of suppressed glomeruli causes a brief increase in high-frequency power initially. This transient is followed by a sustained period of reduced high-frequency fluctuations.

RESULTS

Mapping Mitral/Tufted Cell Excitation and Suppression to Olfactory Bulb Glomeruli

We expressed the genetically encoded calcium reporter GCaMP6f (Chen et al., 2013) selectively in piriform cortex-projecting mitral/tufted (pcMT) cells (see Experimental Procedures) and then imaged evoked fluorescence changes from their apical tufts within dorsal OB glomeruli (Figure 1A). Imaging with two-photon microscopy at relatively low zoom allowed for the visualization of odorant-evoked GCaMP signals in 20–40 glomeruli simultaneously (Figure S1) while restricting optical measurements to the glomerular layer.

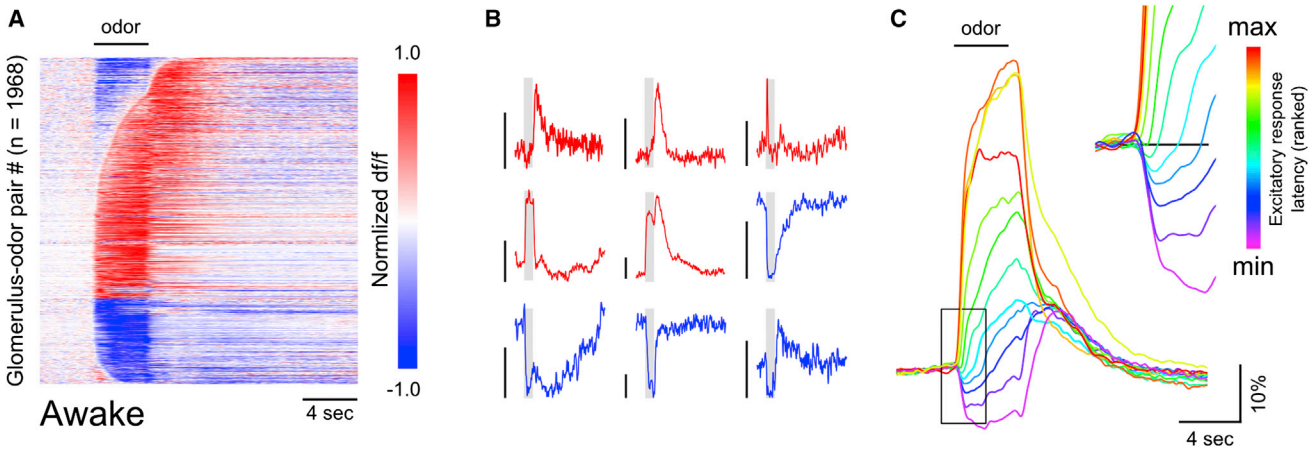

Figure 2. Suppressive Odorant Responses Are Prominent and Impact Response Dynamics among OB Glomeruli in Awake Mice

(A) Response time series across all glomerulus-odorant pairs imaged from pcMTs in glomeruli of awake mice, normalized and plotted as in Figure 1.

(B) Example traces from individual glomerulus-odorant pairs in awake mice. Scale bars, 20% dF/F. Diverse temporal patterning persists in the awake state. Inhalation coupling in awake, freely breathing mice is not evident due to trial averaging and occasional bouts of high-frequency sniffing, which cannot be resolved, due to the insufficient temporal resolution of GCaMP.

(C) Excitatory time series from (A) binned by the latency of the first significant excitatory response, averaged and pseudocolored according to bin. Longer-latency odorant-evoked excitation in pcMT cells is smaller in amplitude and systematically preceded by a period of transient suppression. Following the cessation of odorant application, the average time series of all groups converge to the same trajectory.

In the absence of odorant stimulation, many glomeruli showed slow fluctuations in GCaMP6f fluorescence that varied over timescales of seconds, as well as higher-frequency (>1 Hz) fluctuations (Figures 1B and 1D). The relative power of the high-frequency fluctuations was significantly correlated with the level of the slowly varying "tonic" fluorescence ($r = 0.41$, correlation of tonic fluorescence level with its high-frequency variance, $p < 10^{-142}$), consistent with higher tonic fluorescence levels reflecting higher levels of spontaneous spiking or synaptic input to MT cells. Notably, the presence and time course of these slow fluctuations was glomerulus specific (e.g., Figure 1B). Some glomeruli also showed fluorescence transients linked to each inhalation, even prior to odorant stimulation (Figure 1C), consistent with prior reports of inhalation-driven sensory input to OB glomeruli (Kato et al., 2012; Wachowiak et al., 2013).

Odorant presentation evoked both increases and decreases in GCaMP6f fluorescence that mapped to discrete glomeruli (Figure 1B). Opposing polarity responses to the same odorant were interspersed among glomeruli within a field of view (Figure 1B, right). Responses often consisted of multiphasic sequences of fluorescence increases and decreases linked to odorant onset, offset, and/or inhalation that were specific for a glomerulus-odorant pair and repeatable across presentations (Figures 1B and 1C). Overall, we observed significant fluorescence decreases in 38.4% of all glomerular odorant responses ($n = 2,680$ pairs, 12 mice).

Based on earlier simultaneous recordings of spike rate and GCaMP fluorescence in MT cells (Kato et al., 2012; Wachowiak et al., 2013) and earlier comparisons of calcium signals in the MT soma and apical tuft (Charpak et al., 2001; Debarbieux et al., 2003), the simplest interpretation of these results is that increases and decreases in glomerular GCaMP6f fluorescence reflect increases and decreases, respectively, of ongoing MT cell activity. Consistent with this, glomerular fluorescence decreases were accompanied by a clear suppression of both spontaneous and inhalation-linked transients occurring prior to odorant presentation (Figure 1C), as well as by a marked reduction in the power of spontaneous, higher-frequency fluctuations (Figure 1D).

We next measured odorant-evoked glomerular excitation and suppression during wakefulness by imaging glomerular GCaMP6f signals from pcMTs in awake, head-fixed mice. As observed under anesthesia, stimulation during wakefulness yielded odorant-specific excitatory and suppressive responses in discrete, interspersed glomeruli (Figures 2A and 2B). Odorants evoked net excitatory and suppressive responses with similar probabilities in awake and anesthetized mice (Figure 2A; anesthetized: 38.4%, awake: 35.8%). However, as reported earlier for MT somata (Kato et al., 2012), onset latencies were delayed in awake mice, with approximately 39% of excitatory responses emerging at least one second after the earliest measured response in awake mice, compared to 15% under anesthesia. Notably, longer-latency excitatory responses were preceded by modest suppression of spontaneous GCaMP6 signals (Figures 2A and 2C). These results suggest that, although glomerulus-specific suppression is prominent in both anesthetized and awake mice, additional suppression impacting the temporal evolution of odorant responses during sustained odorant sampling is engaged during wakefulness.

Mitral/Tufted Cell Excitation and Suppression Maps Uniformly onto Glomeruli

To resolve excitation and suppression at the level of single neurons, we next imaged from MT somata at or near the mitral cell layer in anesthetized mice (Figures 3A and 3B). In many MT cells, odorants evoked simple fluorescence increases that included

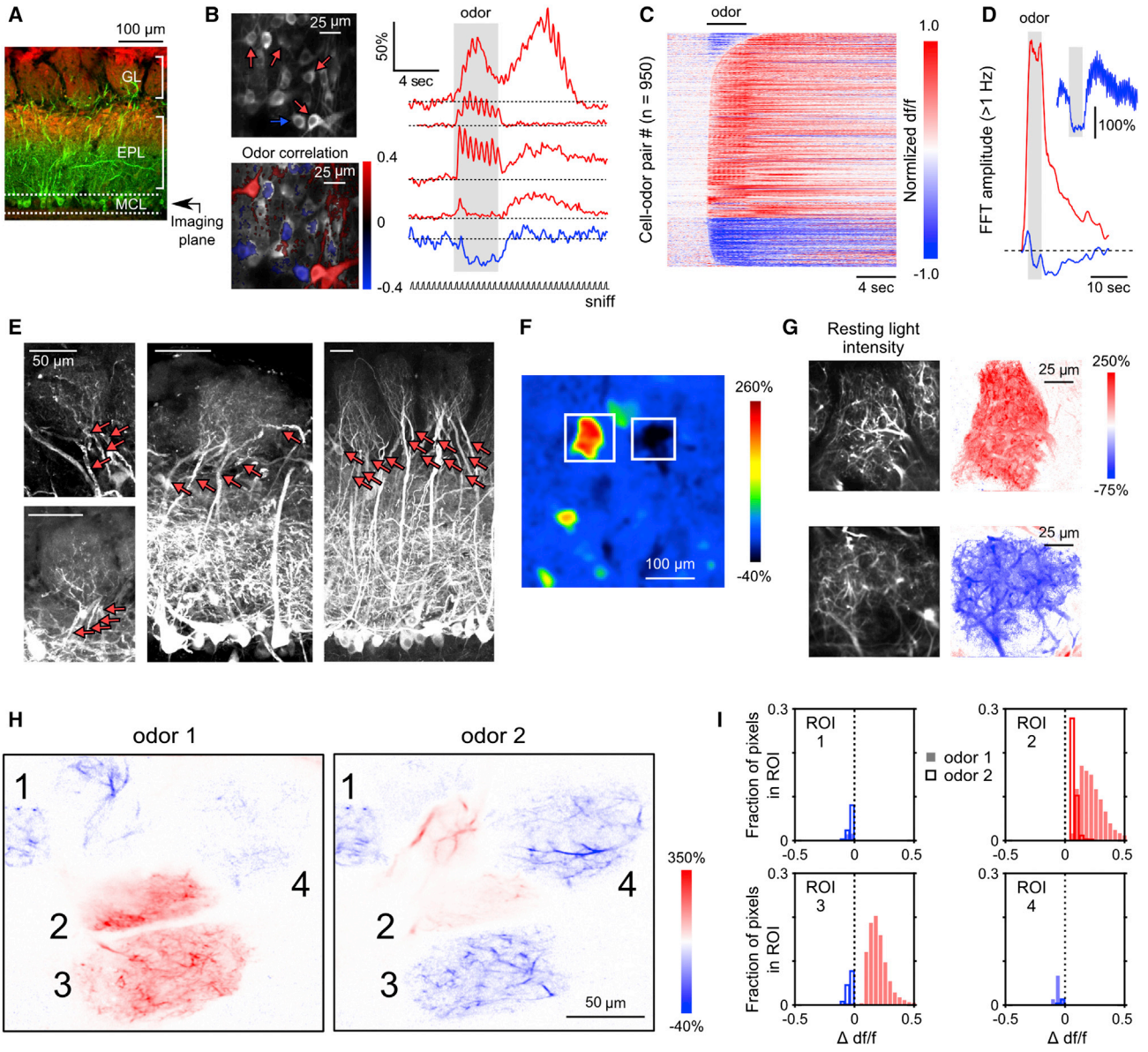

Figure 3. Excitatory and Suppressive Odorant Responses Are Interspersed among pcMT Cell Somata and Are Shared across Sister pcMT Cells in the Same Glomerulus

(A) Reference image indicating imaging plane targeting pcMT somata.

(B) pcMT cells imaged in vivo (top left) and fluorescence time series (right) from select somata showing distinct temporal patterns including fluorescence increases (red) and decreases (blue). Traces are averages of 4 trials. Excited cells with activity positively correlated with odorant presentation were interspersed with negatively correlated (suppressed) cells (different odorant; bottom left). Note that stimulus-activity correlations reveal the polarity of the odorant response but do not quantify similarity between the responses of individual somata.

(C) Odorant-evoked GCaMP signals across a population of cell-odor pairs, displayed as in Figures 1 and 2.

(D) Time course of high-frequency power (summed FFT amplitude > 1 Hz) across all excited (red) and suppressed (blue) somata demonstrates a sustained decrease in high-frequency fluctuations following the initial suppressive transient.

(E) Example confocal images from histological sections showing innervation of glomeruli by multiple pcMT cells. Note that fluorescence is comparatively dim in the glomerular layer. All images show native GCaMP fluorescence with no enhancement by immunostaining.

(F) GCaMP fluorescence imaged from the glomerular layer in vivo illustrating excitation and suppression in two neighboring glomeruli in response to the same odorant (methyl benzoate).

(G). High-resolution imaging from the excited (top) and suppressed (bottom) glomeruli indicated in (F). Left images show individual dendritic processes resolvable within each glomerulus; right images show corresponding pixel-wise df/f maps. All responsive processes within a glomerulus show either a positive (red; excited) or negative (blue; suppressed) response to the odorant.

(legend continued on next page)

inhalation-linked transients, as seen in glomeruli. In other cells, however, responses were more complex and consisted of fluorescence decreases or mixed sequences of increases and decreases that were qualitatively similar to those imaged from glomeruli (Figure 3B, right). The proportion of suppressive responses was moderately smaller than that observed among glomeruli, with 32% of cell-odor pairs (390 pairs, 3 mice) exhibiting a predominate decrease in fluorescence (Figure 3C). The higher proportion of glomeruli showing suppression may follow from the convergence of multiple MT cells onto each glomerulus, with a resulting increase in signal-to-noise ratio arising from averaging across multiple "sister" MT cells. Within a field of view, however, fluorescence increases and decreases (as well as MT somata unresponsive to a given odorant) were interspersed (Figure 3B, left). As with the glomerular signal, somatic fluorescence decreases were typically accompanied by a reduction in the power of high-frequency (>1 Hz) fluctuations (Figure 3D).

How, or whether, MT cell excitation and suppression maps to OB glomeruli—the anatomical units that define odor coding modules within the OB—remains unclear, because MT cells with apical dendrites in the same glomerulus (i.e., "sister" MT cells) may be differentially shaped by inhibitory circuits (Dhawale et al., 2010; Ke et al., 2013). To address this, we imaged at higher magnification to resolve and compare GCaMP6f signals in multiple pcMT dendritic branches within a single glomerulus. Effective retrograde infection of pcMTs results in GCaMP expression in approximately 80% of Tbx21-positive mitral cells (Rothermel et al., 2013); recent studies indicate that individual dorsal OB glomeruli are innervated by 10–20 mitral cells (Ke et al., 2013; Sosulski et al., 2011). Thus, we estimate that most imaged glomeruli included dendrites, conservatively, from 5 to 10 pcMT cells. We confirmed glomerular innervation by multiple GCaMP6-expressing pcMT cells in post hoc histological analysis (Figure 3E) and using high-zoom scans in vivo (Figure S2).

To address whether sister pcMT cells show similar or different response *polarities*, we mapped excitation and suppression across all labeled processes within a glomerulus by calculating, for each responsive pixel, the correlation coefficient between the fluorescence signal extracted from that pixel and the square pulse demarcating the time of odorant presentation (Figures 3F and 3G). Across 115 glomeruli so examined, nearly all stimulus-related pixels within a glomerulus (i.e., those significantly correlated to the stimulus) had correlation coefficients of the same sign (99.8% ± 0.6% of 71.1% ± 28.8% significantly correlated pixels). Even when different odorants evoked excitatory and suppressive responses in the same glomerulus, excitation or suppression was uniform throughout all responsive processes, with a given odorant evoking responses that were either all positive (for excitatory odorants) or all negative (for suppressive odorants) (Figures 3H and 3I; see also Figure S2). In some cases, dendrites within the glomerular neuropil could be putatively assigned to different sister MT cells on the basis of differences in spontaneous activity; in these cases, odorant stimulation nonetheless elicited responses of the same polarity in these cells (Figure S2). Uniform response polarities extended to the apical dendrites of sister MT cells visible outside of the glomerular neuropil (Figure S2).

Overall, these results suggest that inhibition leading to suppression of ongoing activity targets all pcMT cells innervating the same glomerulus. These results do not rule out the possibility that finer-scale differences in response magnitude or temporal dynamics exist between sister pcMT cells or distinct MT subtypes innervating the same glomerulus—as has been shown with electrophysiological recordings and imaging (Dhawale et al., 2010; Kikuta et al., 2013; Tan et al., 2010). However, our data indicate that, at least with respect to response *polarity*, odorant-evoked pcMT responses map uniformly to their parent glomeruli.

The detection of suppressive responses in a glomerulus requires the presence of spontaneous activity in the neurons innervating it. For each glomerulus-odor pair, we calculated an index of spontaneous activity, calculated as the average df/f value immediately prior to odorant presentation normalized by the threshold used to detect significant responses to odorant stimulation. We found that the probability of detecting a suppressive response in a glomerulus depended strongly on this value, which in turn is dependent upon the number of repetitions of each odorant (Figure S3). With eight repetitions, when the mean fluorescence amplitude preceding odorant presentation was at least 2.14 times higher than the significance threshold, the probability of observing a suppressive response was decreased by less than 5% compared to the probability observed in the 10% of cases with the highest spontaneous activity. Spontaneous activity preceding odorant stimulation was at least this high in 86% of all glomerulus-odor pairs. Overall, we estimate that for our dataset only 3.8% of suppressive responses were not detected due to insufficient spontaneous activity in the MT cells innervating each glomerulus (Figure S3), indicating that decreases in activity were reliably identified in this dataset.

Glomerular Output Maps Reveal Odorant-Specific Inhibition of Select Glomeruli

The ability to, for the first time, map MT response patterns across multiple, directly visualized OB glomeruli allows us to characterize the functional organization of excitation and suppression across the glomerular array in vivo. Perhaps the most striking feature of glomerular MT cell responses was their odorant specificity. Examples of glomerular maps evoked by multiple odorants, imaged at different spatial scales in two preparations, are shown in Figures 4A and 4B. In both cases, immediately adjacent glomeruli respond with excitation and suppression to different odorants, and other adjacent glomeruli show no detectable response. Excited, suppressed, and null-responding glomeruli

(H). High-resolution response maps showing resolvable dendritic processes within a group of glomeruli. All dendritic processes within a given glomerulus respond with the same polarity, even for glomeruli that respond with different polarity to different odorants (e.g., glomerulus 3). "Odor 1," ethyl butyrate; "Odor 2," 2-hexanone.

(I) Histograms of changes in df/f values for every significantly modulated pixel within each glomerulus indicated in (H) for two odors (solid bars and open bars). Glomeruli with intermingled excitatory and suppressive responses were never observed.

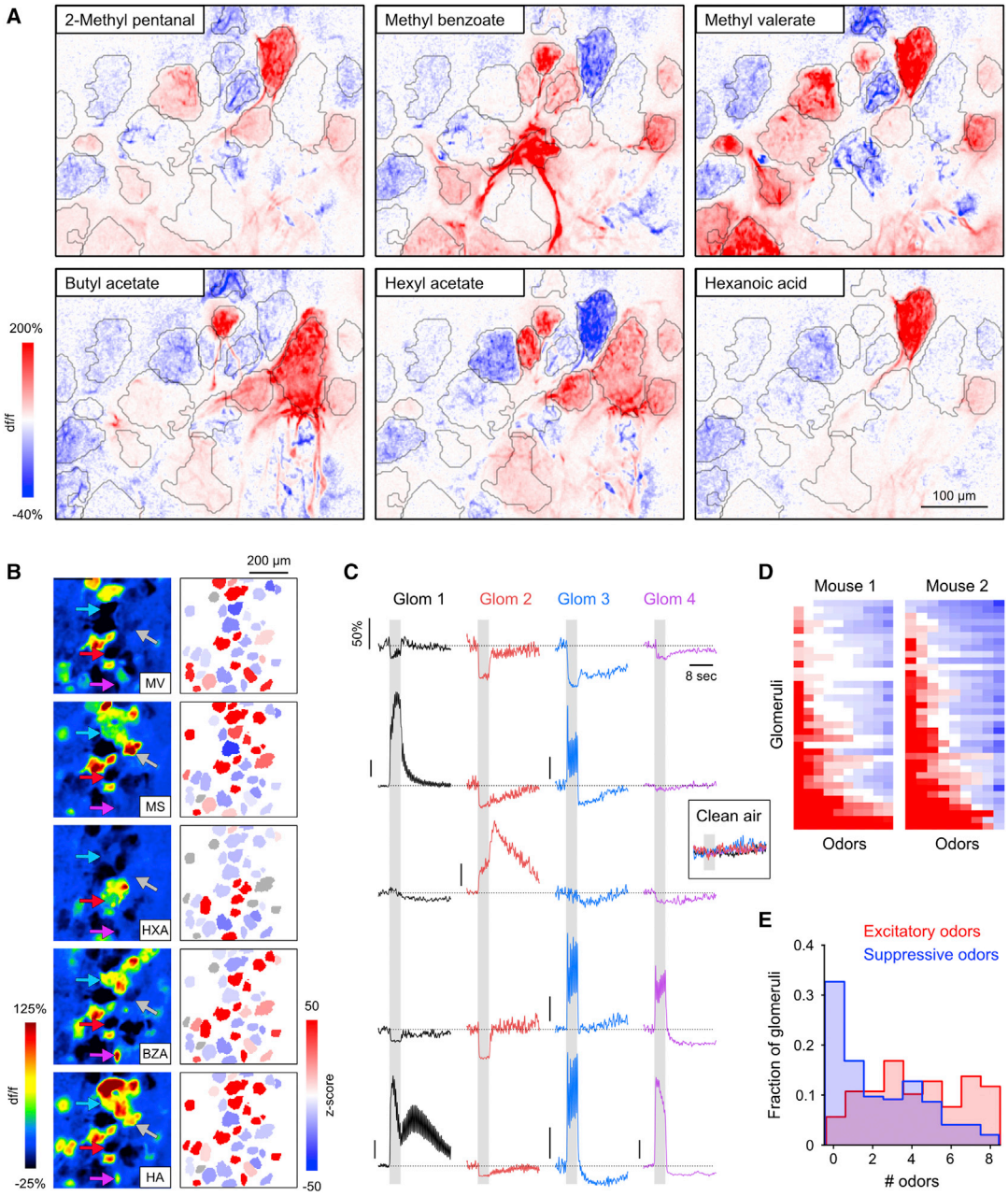

Figure 4. Glomerular Response Polarities Are Highly Interspersed and Odorant Specific

(A) Maps of glomerular MT cell responses (GCaMP6f) evoked by six odorants imaged across the same field of view in an anesthetized mouse. Red and blue indicate fluorescence increases and decreases, respectively. Glomeruli are outlined in gray. Most glomeruli were excited, suppressed, and unresponsive to distinct subsets of the odorant panel.

(B) Glomerular activation maps (left) evoked by five odorants known to strongly activate the dorsal OB, with ROI masks pseudocolored by response *Z* score (right). In all cases, excited (red), suppressed (blue), and non-responsive (gray) glomeruli are intermingled. MV, methyl valerate; MS, methyl salicylate; HXA, hexanoic acid; BZA, benzaldehyde; HA, hexyl acetate.

(C) Time series corresponding to the four glomeruli indicated with arrows in (B) for each of the five odorants. The polarity and time course of each response is glomerulus and odorant specific. Responses were abolished when clean air was used as a stimulus (inset). Scale bar (top left) applies to all traces except where indicated (all represent 50% df/f).

(D) Response matrix representing the strength and polarity of odor-evoked responses in two different mice. Responses were sorted across rows from most excitation to most suppression left to right for ease of visualization. As a result, odorant identity is not preserved across columns. Most glomeruli exhibited excitatory and suppressive responses to subsets of the odorants tested. Odorants not eliciting a detectable response are colored white.

(E) Histogram of the number of odorants eliciting excitation and suppression across all glomeruli, assayed with panels of eight odorants known to strongly activate the dorsal OB.

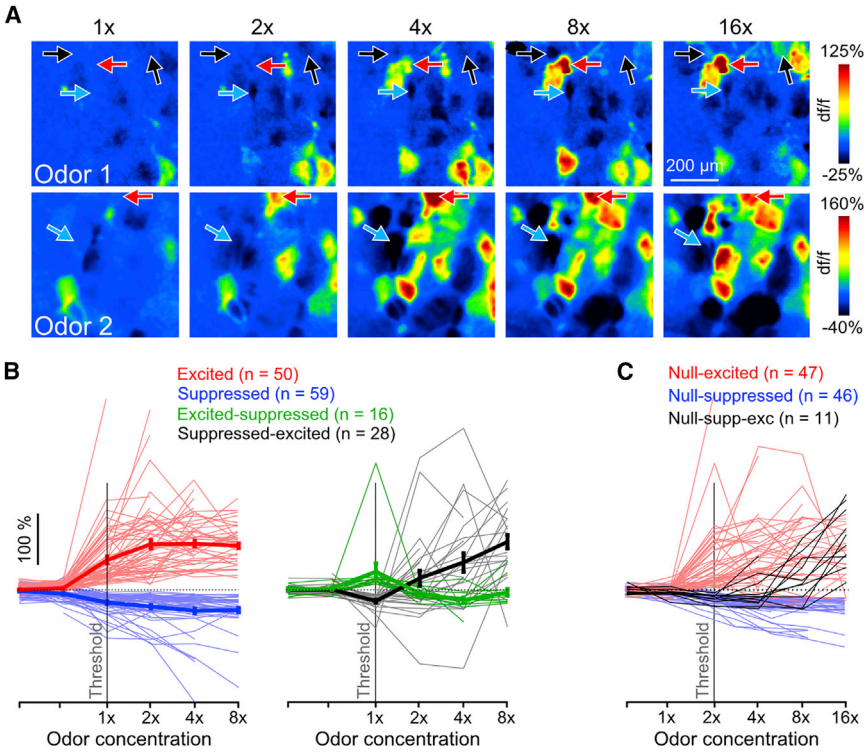

Figure 5. Glomeruli Show Diverse Patterns of pcMT Excitation and Suppression across Odorant Concentration

(A) Pseudocolor df/f maps of glomerular responses to increasing odorant concentration from two representative experiments (Odor 1, ethyl butyrate; Odor 2, methyl valerate). Arrows indicate glomeruli that transition from unresponsive to excitation at higher concentration (red), unresponsive to suppression (blue), and unresponsive to suppression and then to excitation (black).

(B) Responses of all glomeruli to the same odorant across a range of concentrations. The majority of glomeruli responded with the same polarity across all concentrations (71%; 109/153), and are shown in the left plot. Glomeruli showing changes in response polarity with increasing concentration are shown in the right plot. Data points to the left of "1x" represent further decreased concentrations and/or blank stimuli. Dark lines represent mean ± SEM.

(C) Responses of glomeruli exhibiting a null response to at least one low concentration of the odorant. The first suprathreshold response in nearly half of all glomeruli (47/104) was excitatory.

are highly interspersed. The time courses of the glomerular MT responses reveal additional diversity in response patterns that extends beyond simple excitation or suppression to include differences in the temporal response to the onset, duration, and offset of odorant stimulation (Figure 4C). Glomeruli varied greatly in their selectivity for excitatory versus suppressive responses across the odorant panel, with some glomeruli showing broadly tuned excitation and others showing broadly tuned suppression (Figures 4D and 4E). Overall, 66% of glomeruli responded with suppression to at least one of the eight odorants tested. The relative distribution of excitatory versus suppressive MT responses appeared qualitatively similar across animals (n = 18 fields of view imaged from 11 mice; Figure 4D and Figure S4).

How might the specificity in suppression of glomerular output arise from inhibitory OB circuits? Multiple circuits mediate inhibition both within (intraglomerular) and between glomeruli (interglomerular), with distinct predicted impacts on odor representations (Cleland and Linster, 2012; Banerjee et al., 2015). We evaluated the degree to which patterns of glomerular output are consistent with predictions from common interglomerular and intraglomerular circuit models by mapping MT cell excitation and suppression across glomeruli using a panel of odorants, including both structurally similar and divergent compounds that activate glomeruli on the dorsal OB (see Experimental Procedures).

Intensity-Dependent Intraglomerular Inhibition

Odorant-specific suppression of glomerular output could result from a differential sensitivity of MT cell inhibition and excitation to input intensity. OB slice experiments have identified a feedforward inhibitory circuit in which high-sensitivity periglomerular interneurons are recruited at lower input intensities than MT cells, resulting in a predicted suppression of MT output for weak OSN activation and a shift to MT excitation at higher input intensities (Cleland and Linster, 2012; Gire and Schoppa, 2009).

We tested the degree to which suppressive responses could be accounted for by this model by imaging responses from the same glomerulus across an up to 32-fold change in odorant concentration (typical, 16-fold). A signature of the high-sensitivity feedforward inhibition model is the transition of suppressive MT responses into excitatory responses as odorant concentration increases; this model also predicts that the opposite transition—from excitation to suppression—should be rare or not observed. Figure 5A shows examples of glomerular pcMT response patterns for a concentration series of two odorants in the same field of view. Individual glomeruli show a range of behaviors as odorant concentration increases. Overall, approximately 20% of glomeruli (18.3%; 28/153 glomeruli in 4 mice) had concentration-response functions consistent with high-sensitivity feedforward inhibition, with suppression at low odorant concentrations that switched to excitation at higher concentrations (Figure 5B, right). A smaller but still substantial fraction (10.5%; 16/153) switched polarity from excitation to suppression (Figure 5B, right). The majority of imaged glomeruli, however (71.3%), maintained their response polarity at all concentrations tested, with an approximately equal fraction showing excitatory and suppressive responses (excitation: 32.7%, suppression: 38.6%; Figure 5B, left).

To ensure that we sampled concentrations across the relevant range for a glomerulus-odorant pair, we also analyzed the subset of glomeruli whose concentration-response functions were bounded by a null response on the low end and an excitatory

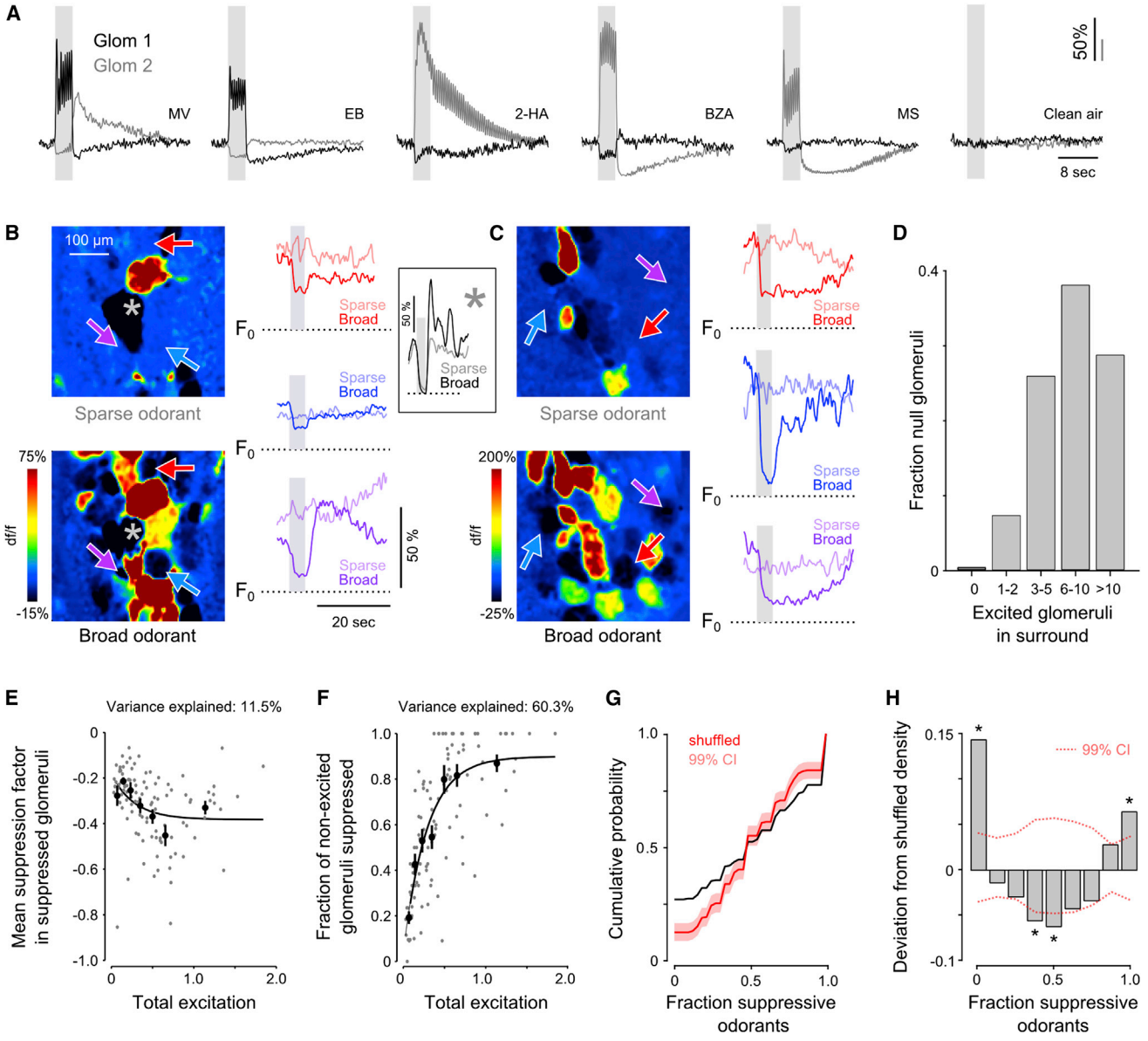

Figure 6. Spatial Patterns of Glomerular Output Do Not Fit a Model of Global Interglomerular Inhibition

(A) Odorant-evoked responses of two glomeruli imaged in the same field of view to five odorants and clean air. Excitation in one glomerulus is accompanied by suppression in the other glomerulus for all five odorants, and vice versa. Other adjacent glomeruli (data not shown) did not show such reciprocal patterns. EB, ethyl butyrate; 2-HA, 2hydroxyacetophenone.

(B) Left: map of responses to an odorant activating few (sparse odorant, pentanal; top) and many glomeruli (broad odorant, ethyl tiglate; bottom). Right: df/f traces corresponding to the three glomeruli indicated by arrows in maps. For each glomerulus, time series are shown in response to the sparse and broad odorants in light and dark colors, respectively. In these examples, df/f traces represent absolute df/f relative to F_0. Inset: df/f recorded in an additional glomerulus (denoted by an asterisk) that was powerfully suppressed by both odorants.

(C) An additional example from a second mouse. Explanation as in (B). Sparse and broad odorants are ethyl butyrate and n-methyl piperidine.

(D) Number of excited glomeruli in the surround (500 µm radius) of null. For 99.6% of null glomeruli, there was at least one excited glomerulus nearby (median = 7.0; 10^{th}–90^{th} percentile = 3–15 excited glomeruli).

(E). Mean magnitude of odorant-evoked suppression across all glomeruli within a field of view plotted as a function of total excitation elicited by that odorant in the same field of view (Supplemental Experimental Procedures). Each gray point is calculated from the responses of all ROIs within a field of view to one odorant; data points were then binned to calculate averages (solid points; mean ± SEM). Solid line shows sigmoidal fit to the binned means. There is only a weak relationship between mean suppression and total excitation.

(F) Probability of observing suppression among all glomeruli in which excitation was not observed, plotted as a function of the total amount of excitation elicited across all glomeruli. Symbols and fit are as in (E).

(legend continued on next page)

response on the high end (Figure 5C). In 81.0% (47/58) of these glomeruli, responses transitioned from no response to excitation with no evidence of intermediate suppression (red) within the resolution of our concentration steps (0.3 log units). We additionally included the population of glomeruli whose responses are bounded below by null responses and are suppressed at all higher concentrations (46 glomeruli) (Figure 5C). Making the very conservative assumption that all of these glomeruli would switch to excitation at a high enough concentration, we still found that among this larger group, nearly half of glomeruli (47/104; 45.2%) did not display suppression at an intermediate concentration. Most glomeruli did display suppression to one or more odorants when tested against a modest odorant panel (e.g., Figures 4D and 4E; Figure S4), implying that suppression is unlikely a simple function of input intensity in many glomeruli. Overall, these results do not exclude the possibility that intraglomerular circuits with differential sensitivity to input strength could contribute to glomerulus-specific suppression. At the same time, they suggest that the high-sensitivity feedforward inhibition model is unlikely to account for all—or even most—instances of odorant-evoked suppression of glomerular output.

Global versus Selective Interglomerular Inhibition

Interglomerular circuits have the potential to mediate glomerulus-specific suppression of MT cell output via lateral inhibition. Consistent with such an organization, we occasionally observed pairs of glomeruli in the same field of view that displayed apparently reciprocal response patterns to an odorant. An example of one such pair is shown in Figure 6A. Excitatory and suppressive components of the MT responses appear reciprocal in each glomerulus, showing roughly inverse responses both across odorants and across time. Such examples are suggestive of mutual inhibitory interactions between glomeruli.

One prevalent interglomerular circuit model involves inhibition that is broadly distributed and scales in magnitude with excitation (Banerjee et al., 2015; Cleland and Sethupathy, 2006). Alternatively, interglomerular inhibition could be selective and spread from an excited glomerulus to a sparse subset of surrounding glomeruli (Fantana et al., 2008; Migliore et al., 2010). To test these models, we analyzed pcMT glomerular responses to single odorants, examining the surround of glomeruli that were unresponsive to an odorant. Surprisingly, we found that these "null" glomeruli could often be found adjacent to strongly excited glomeruli as well as to strongly suppressed glomeruli (Figures 6B and 6C, top maps; Figure S5). Null-responsive glomeruli exhibited high degrees of spontaneous activity (Figures 6B and 6C) and could be suppressed (or excited) reliably by other odorants (Figures 6B and 6C, bottom maps and dark traces). Close appositions of null glomeruli to strongly suppressed glomeruli indicate that null responses were not observed as a result of ubiquitous, but weak, interglomerular inhibition. Many excited glomeruli were typically observed in the surround of null glomeruli (Figure 6D; median = 7.0 excited glomeruli observed within 500 μm). Greater than one-third of null glomeruli had at least one strongly suppressed glomerulus (suppression factor > 0.6) in the same field of view (34.0%; 181/532 glomeruli) and nearly all were located near significantly suppressed glomeruli in which some suppression could be detected (suppression factor > 0.25; 473/532 glomeruli).

These results contrast with predictions from a global inhibition model, in which an odorant that weakly excites only a few glomeruli should elicit relatively weak suppression in surrounding glomeruli, and a strongly excitatory odorant should elicit strong suppression in surrounding—but unexcited—glomeruli. We further evaluated this model by quantitatively analyzing the relationship between the strength of glomerular excitation and the prevalence and magnitude of suppression in glomeruli that were not excited by an odorant (see Supplemental Experimental Procedures). With scaled global inhibition, the strength of inhibition should scale with the strength of excitatory input across glomeruli, while uniformly impacting the glomerular array (Banerjee et al., 2015; Cleland and Sethupathy, 2006). However, we found that while the total observed excitation was highly predictive of the *fraction* of suppressed glomeruli (60.3% of variance explained by sigmoid fit), the *magnitude* of suppression in suppressed glomeruli was only weakly related (11.5% of variance explained) (Figures 6E and 6F). Importantly, the low fraction of suppressed glomeruli evoked by weaker odorants (Figure 6F) does not appear to reflect an "iceberg effect" in which suppression was only detected in the more active glomeruli; spontaneous activity levels in suppressed glomeruli did not vary with the fraction of suppressed glomeruli in the field of view (Figure S6). The lack of a strong relationship between total excitation and suppression strength, along with the commonly observed intermingling of null-responsive, suppressed, and excited glomeruli in an odorant-specific manner, runs counter to predictions from a global interglomerular inhibition model.

Another consequence of nonselective interglomerular inhibition is that if suppression were detected in only a subset of non-excited glomeruli, that subset should be randomly distributed. To test this prediction, we quantified the fraction of non-excitatory odorants (out of an 8-odorant panel) that elicited suppression for each glomerulus in a field of view. Glomerulus-odorant pairs with insufficient spontaneous activity to reliably observe suppression were excluded from this analysis. To determine whether suppressed glomeruli were randomly distributed, we compared the distribution of this measure (n = 252 glomeruli, 9 OBs, 7 mice) with the distributions derived after repeatedly shuffling glomerular identity associated with the responses to each odorant (Figure 6G; see Supplemental Experimental Procedures). The empirical distribution of the fraction of non-excitatory odorants evoking suppression across all glomeruli differed

(G) Cumulative distribution of the fraction of non-excitatory odorants suppressing glomeruli (black line). The cumulative distribution of the same fraction from random data, in which the real responses to each odorant were repeatedly assigned to glomeruli in random order is shown in red. Shaded region represents 99% confidence intervals.

(H) Difference between the probability distributions for the real and shuffled data shown in (G). Dotted lines represent 99% confidence intervals in this difference for the shuffled data. Asterisks denote bins that differed significantly from the shuffled distribution ($p < 0.05$; with Bonferroni correction for multiple comparisons). Glomeruli are more likely to be suppressed by all odorants—or by none—more often than expected by chance.

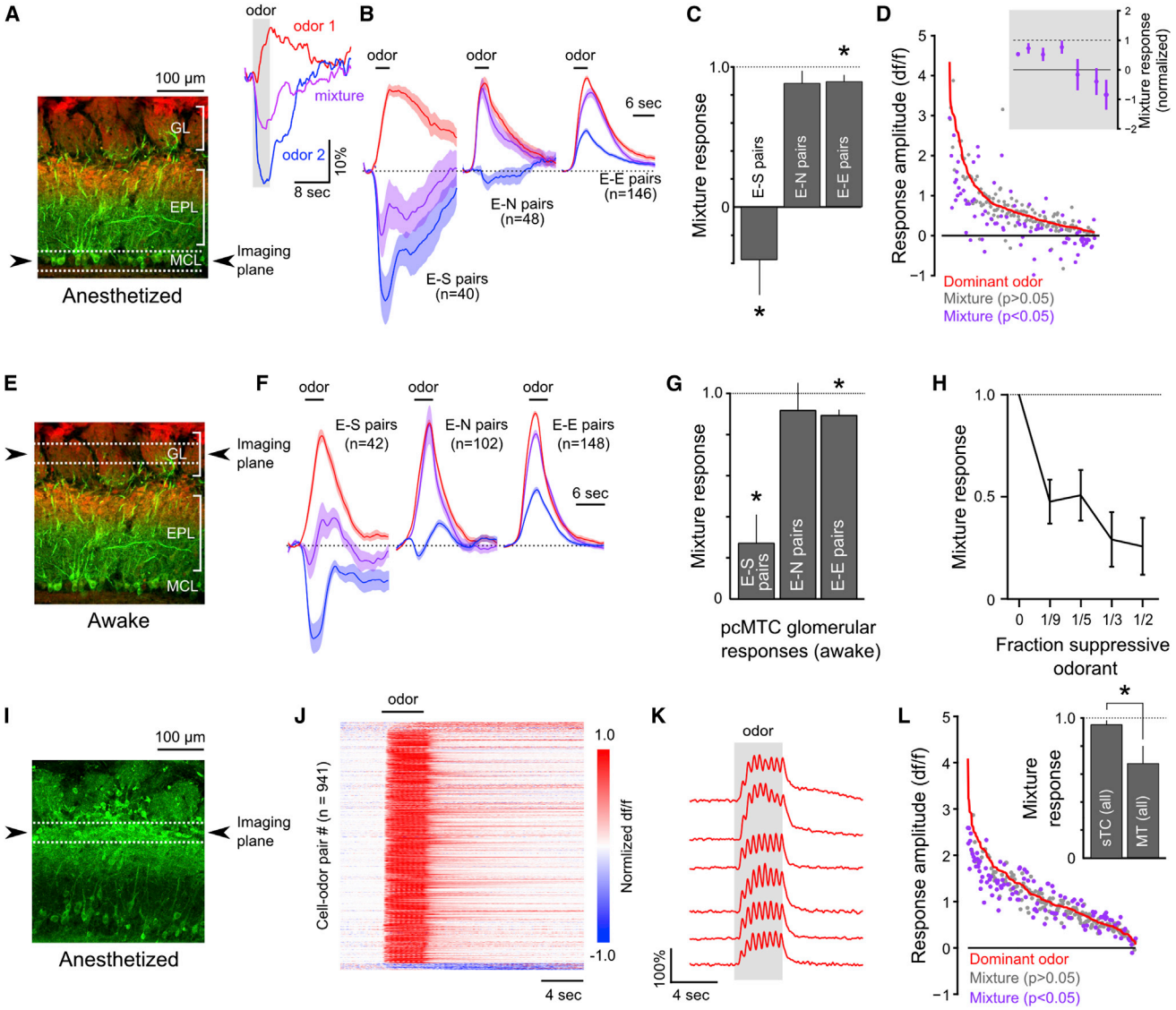

Figure 7. Suppressive Odorants Inhibit Excitation by Other Odorants in Mitral but Not Superficial Tufted Cell Populations

(A) Left: reference image showing schematic of imaging plane, targeting MT cell somata, used for (B)–(D). Inset: example of an MT cell response to an excitatory odorant (red), a suppressive odorant (blue) and their binary mixture (magenta). Traces represent averages of 12 trials.

(B) Time series of mean responses to the dominant odorant (red), weaker odorant (blue), and their binary mixture (magenta) when the weaker odorant was suppressive (E-S pairs), null (E-N pairs), or excitatory (E-E pairs). Time series were normalized by the dominant odorant response amplitude. Shaded areas represent 95% confidence intervals.

(C) Mixture response ratios (mixture response amplitude divided by the dominant odorant response amplitude) for E-E, E-N, and E-S odorant pair types. Bars indicate mean ± SEM. Asterisks denote mixture responses significantly different than 1.0 ($p < 0.05$; uncorrected for multiple comparisons).

(D) Magnitude of odorant-evoked activity in response to the dominant odor (red line) and corresponding mixture responses (points). Cell-odor pairs are rank ordered by the dominant odorant response magnitude on the abscissa. Mixture responses significantly differing from the dominant odorant response are colored magenta. Inset: mean ± SEM of the mixture response ratio of the significantly modulated responses (suppressed or enhanced; binned by rank order on the abscissa) showed suppression of the dominant odorant response, on average, regardless of dominant odorant response magnitude.

(E) Reference image showing schematic of imaging plane for (F)–(H), targeting apical dendritic tufts of MT cells in awake mice.

(F) Mean time series response to the dominant odorant (red), weaker odorant (blue), and their binary mixture (magenta) when the weaker odorant was suppressive (E-S pairs), null (E-N pairs), or excitatory (E-E pairs), as in (B).

(G) Mean mixture response ratios of glomerular responses for E-E, E-N, and E-S odorant pairs, plotted as in (C).

(H) Mixture response ratios of glomerular responses across all E-S pairs at differing concentrations of the suppressive odorant (mean ± SEM). The concentration of the dominant odorant was the same in all cases.

(I) Histological section showing native GCaMP3 fluorescence in deep and superficial tufted cells in a CCK-Cre:Rosa-GCaMP3 reporter cross. Odorant responses were imaged from CCK+ somata near the border of the glomerular and external plexiform layers (dashed lines).

(legend continued on next page)

significantly from the glomerulus-shuffled distribution (Kolmogorov-Smirnov test, $p < 10^{-4}$), indicating that glomeruli are nonrandomly suppressed by odorants. Importantly, the observed and shuffled distributions differed systematically: glomeruli were much more likely than chance to be suppressed either by all or by none of the non-excitatory odorants (Figure 6H). Thus, functional inhibition across the glomerular map depends on glomerular identity, with certain glomeruli subject to more promiscuous functional inhibition than predicted by chance.

Interglomerular Inhibition Shapes the Integration of Odorant Information by MT Cells

The analyses thus far were based on the odorant-evoked suppression of spontaneous activity in MT cell dendrites or somata. To test the degree to which this suppression generalizes to functional inhibition of MT odorant responses—and to further test its interglomerular origin—we used binary odorant mixtures as stimuli. In this paradigm, we compared pcMT responses to each of two test odorants with their response to a binary mixture of the two odorants presented together. We specifically asked whether odorants that evoked suppressive responses when presented individually also suppressed an excitatory response to a different odorant when the two were co-presented in a binary mixture. To quantify mixture interactions, we used a stringent criterion for suppression by an odorant mixture: for a given glomerulus, the response to the mixture had to be significantly smaller than that to the "dominant" (i.e., strongest excitatory) odorant alone (threshold of $p < 0.05$, t test comparing mean excitatory and mixture response amplitudes across 4–16 trials). This criterion—in contrast to a comparison with the sum of the responses to each odorant (Fletcher, 2011; Gupta et al., 2015; Khan et al., 2008)—ensured that mixture suppression represented true inhibition of the response to one odorant by the addition of another, without requiring assumptions about the dynamic range or nature of additivity of inputs to the measured MT cells. To reflect this criterion and to distinguish from the suppression of spontaneous activity evoked by single odorants, we refer to such suppression as "mixture inhibition."

We first examined mixture interactions in pcMT somata expressing GCaMP3 (n = 189 somata, 7 mice) or GCaMP6f (122 somata, 3 mice) in anesthetized mice (Figures 7A–7D). In a given pcMT cell, two odorants could elicit excitatory (E), suppressive (S), or null (N) responses in any combination when presented individually. Among E-S odorant pairs, 56% (24/40 pairs from 10 mice) showed significant mixture inhibition, with the mean response to the mixture showing net suppression below baseline activity (mean = −87% ± 34% of response to excitatory odorant). The remaining 16 E-S pairs, while not significant on a cell-by-cell basis due to across-trial variability, as a population also showed mixture inhibition, with a mean mixture response of 53% ± 32% of the excitatory response amplitude. Indeed, across all 40 E-S odorant pairs, the mean mixture response showed net suppression, equal to −31% ± 26% (mean ± SEM; $p < 10^{-4}$, paired t test) of the response to the excitatory odorant alone (Figures 7B and 7C). The magnitude of mixture inhibition was strongest for pcMT cells with weaker excitatory responses to a single odorant (Figure 7D). We saw much less evidence of mixture inhibition by null odorants, with only 6/48 (12.5%) E-N pairs showing significant inhibition and only slight inhibition of the mean excitatory response across all cell-mixture pairs (mean ± SEM, 86.4% ± 8.8%, $p > 0.05$; Figures 7B and 7C). The relative lack of mixture inhibition observed in E-N pairs suggests that there were few suppressive responses that we failed to detect and misclassified as null. E-E odorant mixtures also produced only a slight reduction in amplitude compared to the dominant odorant (Figures 7B and 7C; mean ± SEM, 89.7% ± 4.7%; $p = 0.02$). These results demonstrate that the suppression evoked by single odorants reflects inhibition that is powerful enough to suppress—and, in many cases, completely block—responses in the same MT cell to excitatory odorants.

We next examined mixture inhibition at the level of glomerular pcMT responses in awake mice (Figures 7E–7H). As seen in pcMT somata, we observed strong mixture inhibition in E-S odorant pairs (Figures 7F and 7G) with a mean mixture response amplitude of 32.6% ± 11.1% of the excitatory odorant (n = 46 pairs; $p < 10^{-9}$, paired t test) and a net reversal of polarity in 18 (of 46) E-S pairs that showed significant mixture inhibition on an individual basis (mixture response amplitude, −32.7% ± 13.3% of excitatory response). Also consistent with the somata imaging, mixture inhibition was significant, but small, in E-E glomerulus-odor pairs (88.2% ± 2.7%; n = 151 pairs; $p < 0.01$) and not significant in E-N pairs (mean, 92.8% ± 15.0%; n = 91 pairs, $p = 0.11$ Figures 7F and 7G).

We further assessed mixture inhibition by imaging glomerular responses to E-S mixtures in which the excitatory and suppressive odorants were mixed at varying ratios (n = 15 odorant pairs in 4 mice). Mixture inhibition was significant even when the proportion of the suppressive odorant was lowered from 50% to 33%, 20%, and 11.1% of the total odorant concentration, while keeping the concentration of the excitatory odorant constant (Figure 7H). The magnitude of mixture suppression decreased somewhat with lower concentration of the suppressive odorant, but remained powerful at the lowest concentration tested (11.1%; 47.7% ± 10.7% of excitatory response; $p < 10^{-4}$, paired t test). Overall, these results support the single-odorant analyses, suggesting that selective interglomerular inhibition strongly regulates odorant-evoked output from OB glomeruli and that mixture effects are not easily explained by intensity-dependent intraglomerular inhibition.

Finally, we tested for mixture inhibition in superficial tufted cells (sTCs), which are reported to be less subject to lateral inhibition than mitral or deep tufted cells (Adam et al., 2014;

(J) Odorant responses measured across a population of superficial tufted cells, plotted as in Figures 1, 2, and 3. Odorant responses were temporally homogeneous compared to MT somata and dendritic tufts. Few suppressive responses were detected in this dataset.

(K) Example responses of a group of simultaneously-imaged superficial tufted cells to an odorant (ethyl butyrate). Odorant responses were typically homogeneous across different cells, limited to the period of odorant stimulation, and highly modulated by sniffing.

(L) Mixture responses, plotted as in (D). Across the population, relatively little modulation by the weak odorant was detected. Inset: Across all somata and odorant pairs, sTCs displayed less mixture inhibition than MT somata. Bars indicate mean ± SEM. Asterisk denotes $p < 0.05$.

Fukunaga et al., 2012; Igarashi et al., 2012; Nagayama et al., 2004). Because tufted, but not mitral, cells express the peptide transmitter cholecystokinin (CCK) (Seroogy et al., 1985), we drove GCaMP3 expression in CCK-positive neurons using the CCK-IRES-Cre (CCK-Cre) and Ai38 Rosa-GCaMP3 reporter mouse strains, and imaging from somata in the superficial external plexiform layer in CCK-Cre:Rosa-GCaMP3 crosses (Figure 7I). With single-odorant stimulation, CCK-positive sTCs showed an apparent lack of suppressive responses. The lack of suppressive responses could reflect a poor ability of GCaMP3 to report suppression; however, sTC responses were also notable in their homogeneous temporal response patterns (Figures 7J and 7K). Importantly, sTCs also showed a distinct lack of suppression by binary mixtures. Across all binary odorant mixtures that included an excitatory odorant (i.e., E-N and E-E mixtures), sTCs showed significantly less mixture inhibition than pcMTs (Figure 7L), with a mean mixture response amplitude of 93.3% ± 3.2% (SEM) of the dominant odorant response for sTCs compared to 66.3% ± 12.7% for all pcMT cells ($p < 0.01$, t test). This result cannot be explained by a difference in the GCaMP variant used, as GCaMP3 has been shown to faithfully follow spike rate above the detection threshold (Wachowiak et al., 2013) and mixture inhibition was apparent using GCaMP3 in pcMT cells. These results also strongly argue against mixture inhibition (or suppression alone) being mediated by peripheral effects such as receptor antagonism and strengthen the notion that sTCs are functionally distinct from both mitral and deep tufted cells in their integration of olfactory stimuli.

DISCUSSION

Synaptic inhibition plays a fundamental role in shaping sensory responses of OB output neurons. Here, using ultrasensitive calcium reporters (Chen et al., 2013), we were able to monitor sensory-evoked excitation and suppression in OB output neurons and to map patterns of excitation and suppression to glomeruli—the functional units underlying odor coding at this level. We found that odorant-evoked inhibition potently suppresses spontaneous and odorant-evoked excitation in MT cells, that suppression of glomerular output is odorant and glomerulus specific, and that inhibition selectively suppresses output from relatively sparse glomerular ensembles. These results point to an unexpected specificity in the distribution of inhibition within and between glomerular modules. They also demonstrate that a fundamental feature of the input-output transformation in the OB is the emergence of odorant- and glomerulus-specific patterns of activity suppression, adding a new dimension over which changes in neural activity can represent odor information.

Imaging from the apical tufts of MT cells allowed us to monitor the activation and suppression of output from discrete glomeruli. We were able to exploit the fact that the apical tuft constitutes the lone site of sensory-evoked excitation onto MT cells, and numerous studies have demonstrated that somatic spikes reliably invade the apical tuft (Bischofberger and Jonas, 1997; Charpak et al., 2001; Debarbieux et al., 2003; Zhou et al., 2006). Thus, it is unlikely that GCaMP fluorescence decreases reflect glomerular inhibition that is not associated with a suppression of spike output. Indeed, a recent study using somatic whole-cell recordings from presumed MT cells in awake animals (Kollo et al., 2014) reported a similar fraction of suppressive odorant responses (46%) as we detected from glomerular tufts in awake (36%) and anesthetized mice (pcMTs: 38%). GCaMP imaging may fail to capture more subtle impacts of inhibition having little impact on time-averaged MT spike rates, such as dendrodendritic signaling from MT cell dendrites and fine-scale temporal firing patterns of MT cells (Fukunaga et al., 2014; Najac et al., 2015; Shao et al., 2012). Nonetheless, our results strongly suggest that odorants evoke specific patterns of inhibition that alter MT cell spike output from select glomeruli.

Temporal response patterns of MT cell excitation and inhibition changed between anesthesia and wakefulness, with an increased prevalence of short-latency odor-evoked inhibition seen in the waking state and, as a result, delayed excitation in a larger fraction of pcMTs. This enhanced short-latency inhibition could explain the sparsening of MT excitatory responses reported in earlier studies in awake mice using extracellular recordings or lower-sensitivity GCaMP reporters and using response measures focused on short-latency responses (Kato et al., 2012; Rinberg et al., 2006; Wachowiak et al., 2013). Our observations also suggest that, during wakefulness, the polarity of an odorant response in a given MT cell could switch from suppressed to excited with sustained sampling (i.e., sniffing)—a behavior that is a hallmark of active odor investigation.

Earlier in vivo studies have inferred the functional organization of inhibition in the OB using single OB neuron recordings and electrical or optogenetic stimulation or optical imaging from undefined neuronal populations (Banerjee et al., 2015; Fantana et al., 2008; Luo and Katz 2001; Ezeh et al., 1993). Several recent studies have proposed that inhibition is broadcast widely from an excitatory locus to surrounding glomeruli, with broad odorant selectivity that scales in magnitude with the overall strength of excitatory input (Banerjee et al., 2015; Cleland and Sethupathy, 2006; Kato et al., 2013). Feedback from piriform cortex may also mediate global inhibition (Boyd et al., 2015). Here, by directly imaging odorant-evoked suppression of MT cell output from individual glomeruli, we found strong evidence that inhibitory OB circuits impact glomerular output in a manner that involves selective inhibitory interactions between OB glomeruli rather than global or center-surround inhibition. First, suppression by single odorants was highly specific across glomeruli in a field of view, even when odorants evoked sparse excitation—a result that we could not explain by differences in spontaneous activity or an inability to detect suppression. Second, the magnitude of suppression in suppressed glomeruli scaled only weakly with total excitation among other glomeruli in the field of view (i.e., Figure 6). Third, in binary mixture experiments, suppressive odorants strongly suppressed excitatory responses from the same glomerulus, but null odorants (which excited nearby glomeruli) did not suppress excitation, nor was suppression seen in mixtures of two excitatory odorants. These results are qualitatively different from those of analogous experiments in piriform cortex, where global inhibition powerfully gates pyramidal cell excitation (Poo and Isaacson, 2009) and mixture suppression is relatively nonspecific (Stettler and Axel, 2009).

How might known inhibitory OB circuits mediate selective suppression of glomerular output? We found that suppression was shared across pcMT cells innervating a glomerulus while selectively targeting particular glomeruli, implicating inhibitory circuits within the glomerular layer. Granule cells may also mediate inhibition of select glomerular modules, and our data do not strictly rule out this possibility. However, a recent study showing that granule cell activation has minimal impact on MT membrane potential or ongoing spike rate (Fukunaga et al., 2014) suggests that it is unlikely that granule cell activity could underlie the silencing of spontaneous fluorescence transients that we observed. In contrast, both intra- and interglomerular inhibitory circuits in the glomerular layer can potently suppress sensory-driven MT spiking in vivo and in OB slices (Aungst et al., 2003; Banerjee et al., 2015; Fukunaga et al., 2014; Gire and Schoppa, 2009; Shao et al., 2012).

Intraglomerular inhibition could mediate odorant-specific suppression of MT output on the basis of a differential sensitivity to input strength; models from OB slice experiments have proposed that periglomerular cells with a lower activation threshold than MT cells drive feedforward inhibition that suppresses MT cell output preferentially at low input intensities, giving way to feedforward excitation at higher input intensities (Cleland and Linster, 2012; Gire and Schoppa, 2009). We observed such concentration-dependent transitions from suppression to excitation in about 20% of cases. However, patterns of glomerular suppression were not broadly consistent with this model. In the binary mixture experiments at the level of both somata and glomeruli, co-presenting an excitatory and suppressive odorant did not lead to greater MT cell excitation as predicted from the high-sensitivity feedforward inhibition model, since presenting the two odorants together would effectively increase ligand concentration and thus input intensity to the parent glomerulus. Likewise, increasing the concentration of the suppressive odorant in the mixture led to more potent suppression rather than less suppression or excitation (e.g., Figure 7H). Thus, while high-sensitivity feedforward intraglomerular inhibition may contribute to odorant-specific patterns of glomerular excitation and suppression, in general our results suggest that MT response polarity is largely determined by odorant identity rather than relative intensity. Feedforward intraglomerular circuits may play other roles in shaping MT cell responses, such as mediating gain control or regulating sensitivity to odorant-evoked excitation; alternatively, intraglomerular inhibition may shape the temporal structure of MT cell responses relative to inhalation or across repeated samples (“sniffs”) of odorant (Najac et al., 2015; Fukunaga et al., 2014; Shao et al., 2012; Wachowiak and Shipley, 2006).

Interglomerular inhibition mediated by short axon cells could mediate the glomerulus-wide suppression that we observed. In this model, short axon cells inhibit external tufted cells located in distant glomeruli (Banerjee et al., 2015; Liu et al., 2013; Whitesell et al., 2013); external tufted cells drive excitation throughout the glomerulus, and thus their inhibition would be expected to suppress spontaneous and sensory-evoked spiking in MT cells with apical tufts in the same glomerulus (Hayar et al., 2004). How the short axon cell networks could mediate inhibition of odorant-specific glomerular ensembles is less clear, however. Short axon cells arising from a single glomerulus project widely to many neighboring glomeruli (Kiyokage et al., 2010), and focal optical stimulation of short axon cells in vivo drives widespread suppression of MT cell spiking (Banerjee et al., 2015). We found, however, that odorant stimulation led to highly selective suppression or excitation of MT output in a cohort of adjacent glomeruli. If short axon cells mediate interglomerular inhibition, a key question is how this inhibition can mediate MT cell suppression with such selectivity. One possibility is that the network of short axon cells broadcasting inhibition from one glomerulus to others is widespread but heterogeneous and relatively sparse in its innervation of surrounding glomeruli, such that each glomerulus receives short axon cell-mediated inhibition originating from a unique combination of neighbors. As a result, the strength of interglomerular inhibition targeting each glomerulus could be a combinatorial function of the strength of excitation among the cohort of surrounding glomeruli. Anatomical descriptions of short axon cell branching patterns are consistent with this model (Kiyokage et al., 2010), but higher-resolution anatomical and functional mapping studies are required to further support or reject it.

A key next step is understanding the organization of selective interglomerular inhibition with respect to odor coding space. We found evidence that this organization is nonrandom, with a subset of glomeruli being suppressed by many more odorants than predicted by chance and another subset showing little suppression. Whether this nonrandom structure is stereotyped between glomeruli representing the same odorant receptor in different individuals, reflects the odorant response properties of incoming sensory neurons (Linster et al., 2005), or is determined by odor experience remains to be determined. The ability to map activity to defined neuronal populations within OB glomeruli and, ultimately, to odorant receptor identity in vivo should enable an understanding of the functional logic by which inhibition targets specific glomerular modules.

EXPERIMENTAL PROCEDURES

Details of all procedures are provided in the Supplemental Experimental Procedures. Briefly, experiments were performed on male and female mice expressing Cre recombinase (Cre) in defined neuronal populations. The mouse strains used were: PCdh21-Cre (Nagai et al., 2005), Ai38 (Zariwala et al., 2012), and CCK-IRES-Cre (Jackson Labs). Cre-dependent expression of GCaMP3 or GCaMP6f in MT cells was achieved by crossing with the Ai38 GCaMP3 reporter line (for CCK-IRES-Cre mice) or by injection of viral vectors as described previously (Wachowiak et al., 2013). In vivo two-photon imaging was performed as described previously (Wachowiak et al., 2013) under pentobarbital or isoflurane anesthesia or in awake mice. No difference in response properties measured under the two anesthetics were observed, and so data from both conditions were pooled. To control inhalation timing, we tracheotomized mice and used artificial inhalation to decouple breathing and odorant stimulation in anesthetized mice (Wachowiak and Cohen, 2001). For imaging in awake mice, animals were acclimated for at least two 30 min sessions prior to data collection.

SUPPLEMENTAL INFORMATION

Supplemental Information includes Supplemental Experimental Procedures and six figures and can be found with this article online at http://dx.doi.org/10.1016/j.neuron.2016.06.001.

AUTHOR CONTRIBUTIONS

Conceptualization, M.N.E. and M.W.; Methodology, M.N.E. and M.W.; Investigation, M.N.E., K.R.H., and M.W.; Data Curation, M.N.E.; Writing – Original Draft, M.N.E. and M.W; Writing – Review & Editing, M.N.E., K.R.H., and M.W; Funding Acquisition, M.N.E. and M.W.

ACKNOWLEDGMENTS

We thank Tom Bozza for providing the M72-ChR2 mouse line used in the Supplemental Information and for advice on odorant panels. We also thank Christine Zabawa, Jackson Ball, and Thomas Rust for technical assistance; Markus Rothermel, Daniela Brunert, Marta Diaz-Quesada, Thomas Eiting, Yusuke Tsuno, Isaac Youngstrom, and Andrew Moran for sharing materials and expertise; and Fernando Fernandez, Michael Shipley, and M.W. lab members for helpful discussion and comments on the manuscript. Funding was provided by NIH (R01 DC06441 to M.W. and F32 DC012718 to M.N.E.) and the University of Utah Office of Undergraduate Research (to K.R.H.).

Received: December 1, 2014
Revised: October 30, 2015
Accepted: May 25, 2016
Published: June 23, 2016

REFERENCES

Adam, Y., Livneh, Y., Miyamichi, K., Groysman, M., Luo, L., and Mizrahi, A. (2014). Functional transformations of odor inputs in the mouse olfactory bulb. Front. Neural Circuits *8*, 129.

Aungst, J.L., Heyward, P.M., Puche, A.C., Karnup, S.V., Hayar, A., Szabo, G., and Shipley, M.T. (2003). Centre-surround inhibition among olfactory bulb glomeruli. Nature *426*, 623–629.

Banerjee, A., Marbach, F., Anselmi, F., Koh, M.S., Davis, M.B., Garcia da Silva, P., Delevich, K., Oyibo, H.K., Gupta, P., Li, B., and Albeanu, D.F. (2015). An interglomerular circuit gates glomerular output and implements gain control in the mouse olfactory bulb. Neuron *87*, 193–207.

Bischofberger, J., and Jonas, P. (1997). Action potential propagation into the presynaptic dendrites of rat mitral cells. J. Physiol. *504*, 359–365.

Boyd, A.M., Kato, H.K., Komiyama, T., and Isaacson, J.S. (2015). Broadcasting of cortical activity to the olfactory bulb. Cell Rep. *10*, 1032–1039.

Charpak, S., Mertz, J., Beaurepaire, E., Moreaux, L., and Delaney, K. (2001). Odor-evoked calcium signals in dendrites of rat mitral cells. Proc. Natl. Acad. Sci. USA *98*, 1230–1234.

Chen, T.-W., Wardill, T.J., Sun, Y., Pulver, S.R., Renninger, S.L., Baohan, A., Schreiter, E.R., Kerr, R.A., Orger, M.B., Jayaraman, V., et al. (2013). Ultrasensitive fluorescent proteins for imaging neuronal activity. Nature *499*, 295–300.

Cleland, T.A., and Linster, C. (2012). On-center/inhibitory-surround decorrelation via intraglomerular inhibition in the olfactory bulb glomerular layer. Front. Integr. Nuerosci. *6*, 5.

Cleland, T.A., and Sethupathy, P. (2006). Non-topographical contrast enhancement in the olfactory bulb. BMC Neurosci. *7*, 7.

Debarbieux, F., Audinat, E., and Charpak, S. (2003). Action potential propagation in dendrites of rat mitral cells in vivo. J. Neurosci. *23*, 5553–5560.

Dhawale, A.K., Hagiwara, A., Bhalla, U.S., Murthy, V.N., and Albeanu, D.F. (2010). Non-redundant odor coding by sister mitral cells revealed by light addressable glomeruli in the mouse. Nat. Neurosci. *13*, 1404–1412.

Ezeh, P.I., Wellis, D.P., and Scott, J.W. (1993). Organization of inhibition in the rat olfactory bulb external plexiform layer. J. Neurophysiol. *70*, 263–274.

Fantana, A.L., Soucy, E.R., and Meister, M. (2008). Rat olfactory bulb mitral cells receive sparse glomerular inputs. Neuron *59*, 802–814.

Fletcher, M.L. (2011). Analytical processing of binary mixture information by olfactory bulb glomeruli. PLoS ONE *6*, e29360.

Fukunaga, I., Berning, M., Kollo, M., Schmaltz, A., and Schaefer, A.T. (2012). Two distinct channels of olfactory bulb output. Neuron *75*, 320–329.

Fukunaga, I., Herb, J.T., Kollo, M., Boyden, E.S., and Schaefer, A.T. (2014). Independent control of gamma and theta activity by distinct interneuron networks in the olfactory bulb. Nat. Neurosci. *17*, 1208–1216, advance online publication.

Gire, D.H., and Schoppa, N.E. (2009). Control of on/off glomerular signaling by a local GABAergic microcircuit in the olfactory bulb. J. Neurosci. *29*, 13454–13464.

Gupta, P., Albeanu, D.F., and Bhalla, U.S. (2015). Olfactory bulb coding of odors, mixtures and sniffs is a linear sum of odor time profiles. Nat. Neurosci. *18*, 272–281, advance online publication.

Hayar, A., Karnup, S., Ennis, M., and Shipley, M.T. (2004). External tufted cells: a major excitatory element that coordinates glomerular activity. J. Neurosci. *24*, 6676–6685.

Igarashi, K.M., Ieki, N., An, M., Yamaguchi, Y., Nagayama, S., Kobayakawa, K., Kobayakawa, R., Tanifuji, M., Sakano, H., Chen, W.R., and Mori, K. (2012). Parallel mitral and tufted cell pathways route distinct odor information to different targets in the olfactory cortex. J. Neurosci. *32*, 7970–7985.

Isaacson, J.S., and Scanziani, M. (2011). How inhibition shapes cortical activity. Neuron *72*, 231–243.

Kato, H.K., Chu, M.W., Isaacson, J.S., and Komiyama, T. (2012). Dynamic sensory representations in the olfactory bulb: modulation by wakefulness and experience. Neuron *76*, 962–975.

Kato, H.K., Gillet, S.N., Peters, A.J., Isaacson, J.S., and Komiyama, T. (2013). Parvalbumin-expressing interneurons linearly control olfactory bulb output. Neuron *80*, 1218–1231.

Ke, M.-T., Fujimoto, S., and Imai, T. (2013). SeeDB: a simple and morphology-preserving optical clearing agent for neuronal circuit reconstruction. Nat. Neurosci. *16*, 1154–1161.

Khan, A.G., Thattai, M., and Bhalla, U.S. (2008). Odor representations in the rat olfactory bulb change smoothly with morphing stimuli. Neuron *57*, 571–585.

Kikuta, S., Fletcher, M.L., Homma, R., Yamasoba, T., and Nagayama, S. (2013). Odorant response properties of individual neurons in an olfactory glomerular module. Neuron *77*, 1122–1135.

Kiyokage, E., Pan, Y.-Z., Shao, Z., Kobayashi, K., Szabo, G., Yanagawa, Y., Obata, K., Okano, H., Toida, K., Puche, A.C., and Shipley, M.T. (2010). Molecular identity of periglomerular and short axon cells. J. Neurosci. *30*, 1185–1196.

Kollo, M., Schmaltz, A., Abdelhamid, M., Fukunaga, I., and Schaefer, A.T. (2014). 'Silent' mitral cells dominate odor responses in the olfactory bulb of awake mice. Nat. Neurosci. *17*, 1313–1315.

Linster, C., Sachse, S., and Galizia, C.G. (2005). Computational modeling suggests that response properties rather than spatial position determine connectivity between olfactory glomeruli. J. Neurophysiol. *93*, 3410–3417.

Liu, S., Plachez, C., Shao, Z., Puche, A., and Shipley, M.T. (2013). Olfactory bulb short axon cell release of GABA and dopamine produces a temporally biphasic inhibition-excitation response in external tufted cells. J. Neurosci. *33*, 2916–2926.

Luo, M., and Katz, L.C. (2001). Response correlation maps of neurons in the mammalian olfactory bulb. Neuron *32*, 1165–1179.

Migliore, M., Hines, M.L., McTavish, T.S., and Shepherd, G.M. (2010). Functional roles of distributed synaptic clusters in the mitral-granule cell network of the olfactory bulb. Front. Integr. Nuerosci. *4*, 122.

Nagai, Y., Sano, H., and Yokoi, M. (2005). Transgenic expression of Cre recombinase in mitral/tufted cells of the olfactory bulb. Genesis *43*, 12–16.

Nagayama, S., Takahashi, Y.K., Yoshihara, Y., and Mori, K. (2004). Mitral and tufted cells differ in the decoding manner of odor maps in the rat olfactory bulb. J. Neurophysiol. *91*, 2532–2540.

Najac, M., Sanz Diez, A., Kumar, A., Benito, N., Charpak, S., and De Saint Jan, D. (2015). Intraglomerular lateral inhibition promotes spike timing variability in principal neurons of the olfactory bulb. J. Neurosci. *35*, 4319–4331.

Poo, C., and Isaacson, J.S. (2009). Odor representations in olfactory cortex: "sparse" coding, global inhibition, and oscillations. Neuron *62*, 850–861.

Rinberg, D., Koulakov, A., and Gelperin, A. (2006). Sparse odor coding in awake behaving mice. J. Neurosci. *26*, 8857–8865.

Rothermel, M., Brunert, D., Zabawa, C., Díaz-Quesada, M., and Wachowiak, M. (2013). Transgene expression in target-defined neuron populations mediated by retrograde infection with adeno-associated viral vectors. J. Neurosci. *33*, 15195–15206.

Seroogy, K.B., Brecha, N., and Gall, C. (1985). Distribution of cholecystokinin-like immunoreactivity in the rat main olfactory bulb. J. Comp. Neurol. *239*, 373–383.

Shao, Z., Puche, A.C., Kiyokage, E., Szabo, G., and Shipley, M.T. (2009). Two GABAergic intraglomerular circuits differentially regulate tonic and phasic presynaptic inhibition of olfactory nerve terminals. J. Neurophysiol. *101*, 1988–2001.

Shao, Z., Puche, A.C., Liu, S., and Shipley, M.T. (2012). Intraglomerular inhibition shapes the strength and temporal structure of glomerular output. J. Neurophysiol. *108*, 782–793.

Shao, Z., Puche, A.C., and Shipley, M.T. (2013). Intraglomerular inhibition maintains mitral cell response contrast across input frequencies. J. Neurophysiol. *110*, 2185–2191.

Sosulski, D.L., Bloom, M.L., Cutforth, T., Axel, R., and Datta, S.R. (2011). Distinct representations of olfactory information in different cortical centres. Nature *472*, 213–216.

Stettler, D.D., and Axel, R. (2009). Representations of odor in the piriform cortex. Neuron *63*, 854–864.

Tan, J., Savigner, A., Ma, M., and Luo, M. (2010). Odor information processing by the olfactory bulb analyzed in gene-targeted mice. Neuron *65*, 912–926.

Wachowiak, M., and Cohen, L.B. (2001). Representation of odorants by receptor neuron input to the mouse olfactory bulb. Neuron *32*, 723–735.

Wachowiak, M., and Shipley, M.T. (2006). Coding and synaptic processing of sensory information in the glomerular layer of the olfactory bulb. Semin. Cell Dev. Biol. *17*, 411–423.

Wachowiak, M., Economo, M.N., Díaz-Quesada, M., Brunert, D., Wesson, D.W., White, J.A., and Rothermel, M. (2013). Optical dissection of odor information processing in vivo using GCaMPs expressed in specified cell types of the olfactory bulb. J. Neurosci. *33*, 5285–5300.

Whitesell, J.D., Sorensen, K.A., Jarvie, B.C., Hentges, S.T., and Schoppa, N.E. (2013). Interglomerular lateral inhibition targeted on external tufted cells in the olfactory bulb. J. Neurosci. *33*, 1552–1563.

Yokoi, M., Mori, K., and Nakanishi, S. (1995). Refinement of odor molecule tuning by dendrodendritic synaptic inhibition in the olfactory bulb. Proc. Natl. Acad. Sci. USA *92*, 3371–3375.

Zariwala, H.A., Borghuis, B.G., Hoogland, T.M., Madisen, L., Tian, L., De Zeeuw, C.I., Zeng, H., Looger, L.L., Svoboda, K., and Chen, T.-W. (2012). A Cre-dependent GCaMP3 reporter mouse for neuronal imaging in vivo. J. Neurosci. *32*, 3131–3141.

Zhou, Z., Xiong, W., Zeng, S., Xia, A., Shepherd, G.M., Greer, C.A., and Chen, W.R. (2006). Dendritic excitability and calcium signalling in the mitral cell distal glomerular tuft. Eur. J. Neurosci. *24*, 1623–1632.

Neuron, Volume *91*

Supplemental Information

Control of Mitral/Tufted Cell Output by Selective Inhibition among Olfactory Bulb Glomeruli

Michael N. Economo, Kyle R. Hansen, and Matt Wachowiak

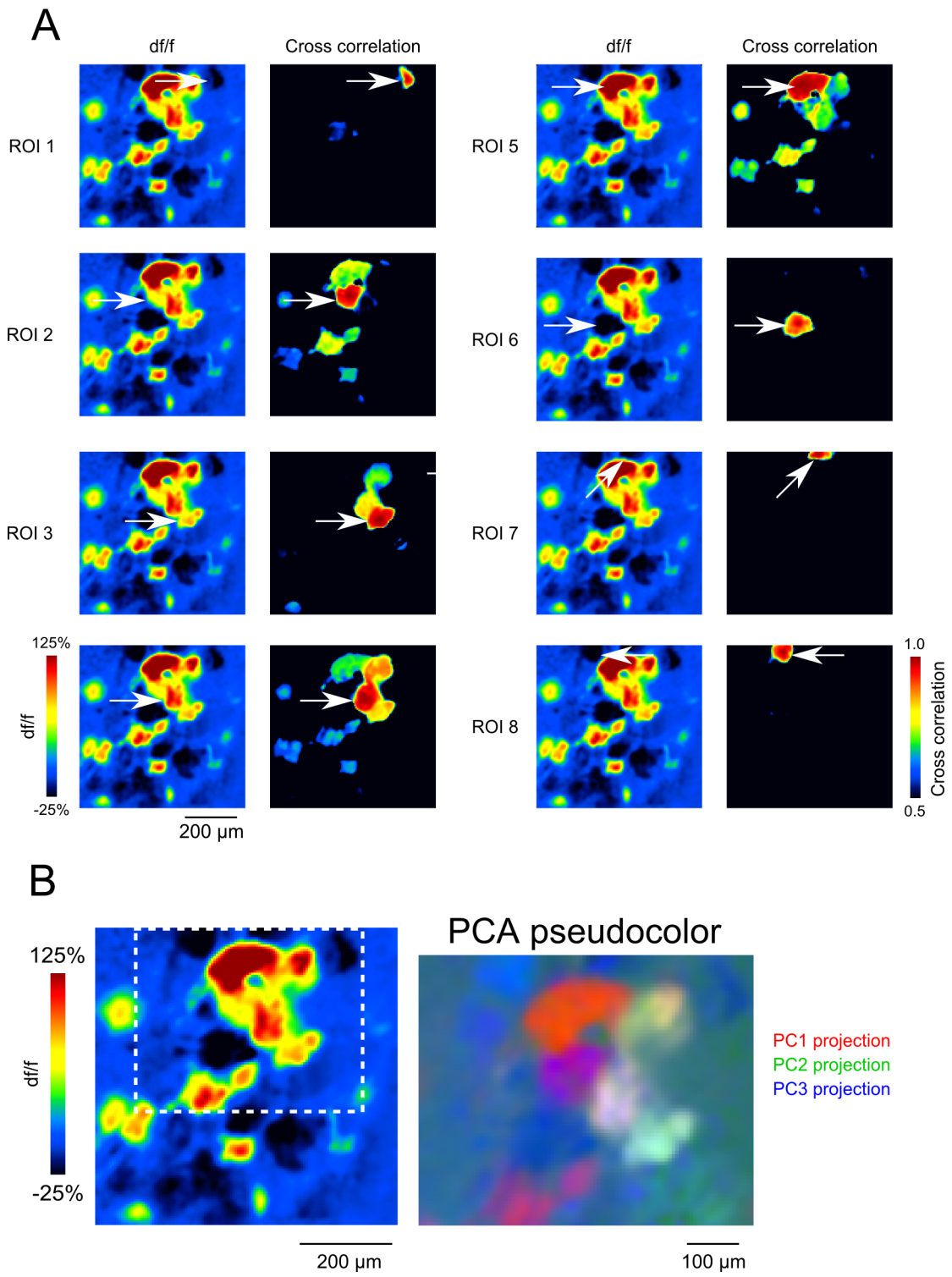

Figure S1 (related to Figure 1). Activity-based identification of glomeruli.

A. Left images: df/f response maps to the odorant hexyl acetate. White arrow in each image indicates the position of a small seed ROI. Right images: Cross correlation values between the time-series of each pixel in an image and the time series extracted from the seed ROI. Cross-correlation maps reveal isolated glomeruli.
B. The response map from A contains a cluster of activated and closely spaced glomeruli. Performing principal component analysis on a subset of the image containing this cluster (dotted white line, left) and mapping the projections onto the first three components onto the colors red, green, and blue reveals groups of pixels with similar time courses (and thus colored with similar hues) corresponding to single glomeruli and provides further confirmation that identified ROIs correspond to discrete glomeruli.

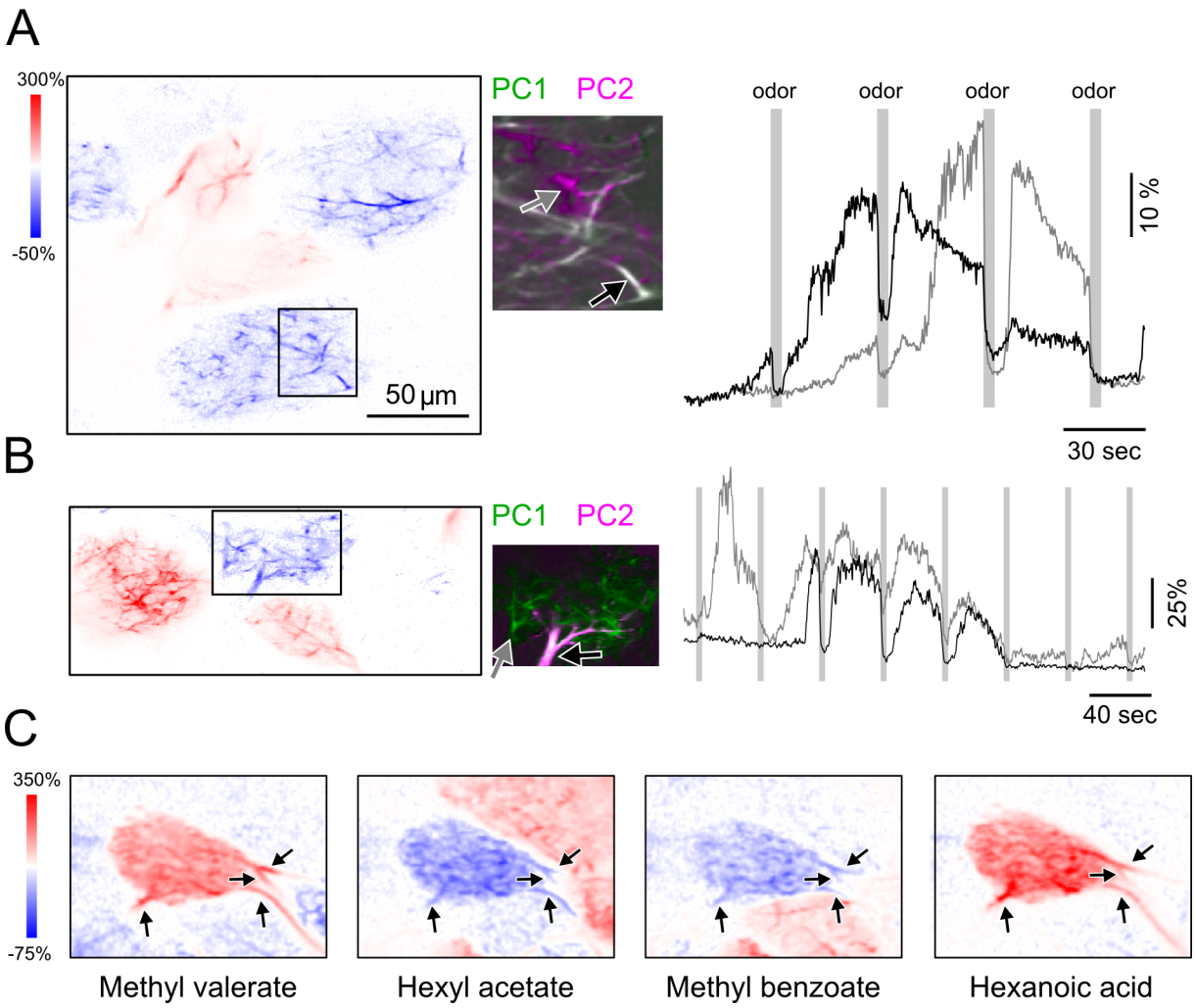

Figure S2 (related to Figure 3). Activity measurements in multiple dendritic segments within single glomeruli.

A. Left: Odorant response map of several adjacent glomeruli (same example is shown in figure 3H). Region demarcated by box expanded (middle) and color coded according to a projection onto the first two principal components extracted from odorant stimulation time series. Dendritic segments putatively originating from two different sister MT cells appear as white/magenta (components scaled arbitrarily for contrast). Time-series extracted from ROIs corresponding to the white/magenta dendrites (black/gray arrows) are represented by black/gray traces (right).
B. Additional example from a different animal in which two intermingled dendritic tufts with unique activity patterns can be isolated within the glomerular neuropil. Color codes are the same as in (A). In both examples, intermingled dendrites have the same response polarity but display different patterns of spontaneous activity.
C. High-zoom response map of the same glomerulus to four odorants (two excitatory and two suppressive). Arrows indicate segments of four apical dendrites innervating the glomerulus that all show the same response polarity to each odorant.

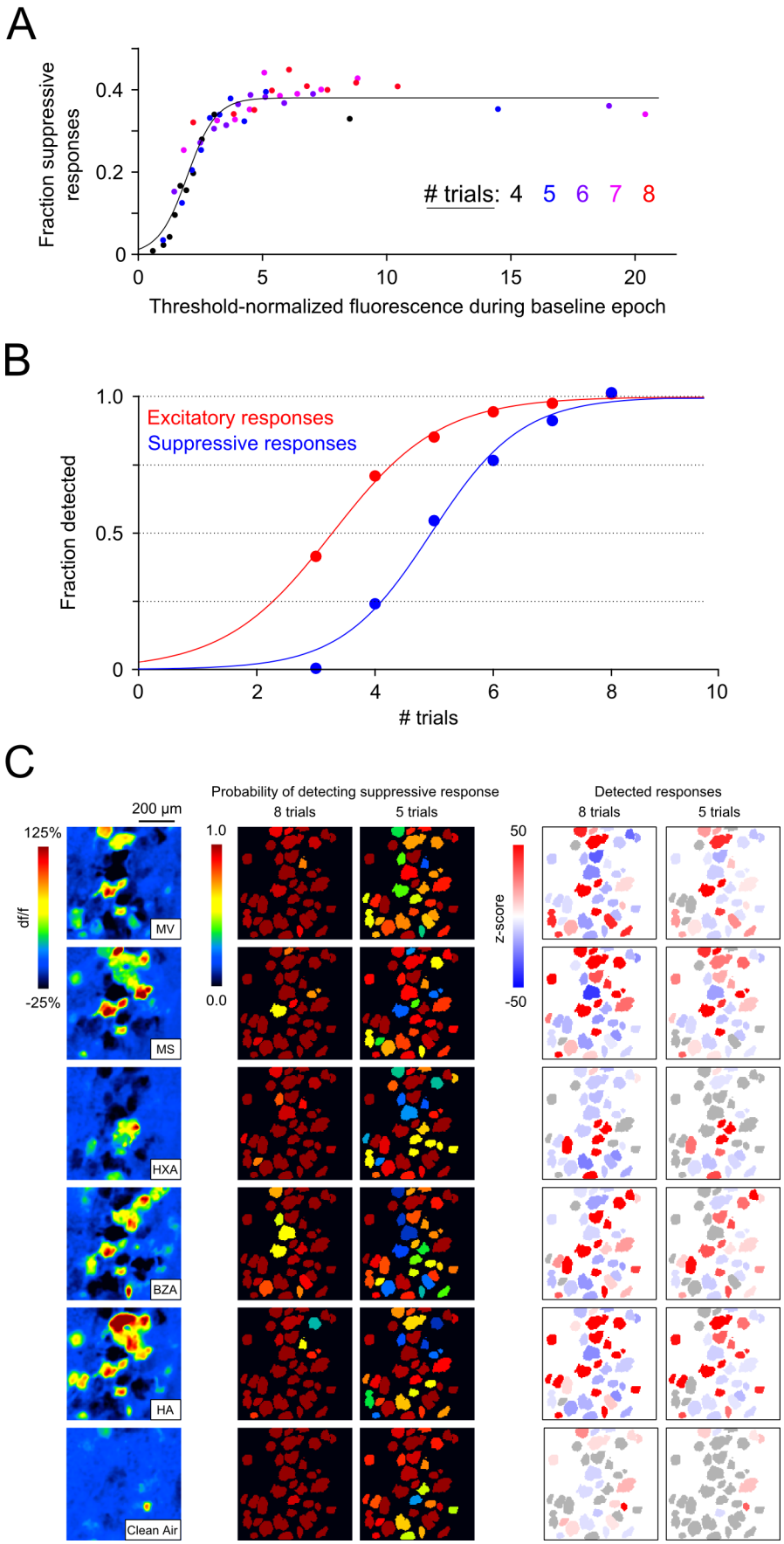
A
Fraction suppressive responses
0.4
0.2
0
trials: 4 5 6 7 8
0
5
10
15
20
Threshold-normalized fluorescence during baseline epoch
B
Fraction detected
1.0
0.5
0
Excitatory responses
Suppressive responses
0
2
4
6
8
10
trials
C
200 µm
Probability of detecting suppressive response
8 trials
5 trials
Detected responses
8 trials
5 trials
125%
df/f
-25%
1.0
0.0
50
z-score
-50
MV
MS
HXA
BZA
HA
Clean Air

Figure S3 (related to Figure 4). Levels of spontaneous activity in the majority of glomeruli are sufficient for detecting suppressive responses.

A. The probability of detecting a suppressive response was closely related to the fluorescence amplitude preceding odorant presentation. Red points: 2680 glomerulus-odor pairs were binned according to their mean pre-odor df/f across 8 odorant presentations. The value on the abscissa represents the pre-odor df/f normalized by the significance threshold used to detect changes in df/f relative to the pre-odor period. In each bin, the fraction of responses classified as suppressive was calculated and corresponds to the value on the ordinate. Other points: The dataset was randomly subsampled to include only a subset of trials in order to artificially reduce statistical power. This shifts the location of the bin centers to the left and reduces the fraction of detected responses. A sigmoidal fit to all of the data is shown in black.

B. Estimated fraction of detected suppressive and excitatory responses with differing numbers of stimulus presentations. Both curves were normalized to the asymptotic value of the sigmoidal fit.

C. Left: df/f maps in response to five odorants and clean air. Same data as in Figure 4. Middle: ROI masks corresponding to individual glomeruli color-coded by the probability of observing a suppressive response normalized to the asymptotic value in (B). Suppressive response detection probabilities were only diminished in a small subset of glomerulus-odor pairs when stimuli were repeated 8 times, while detection probabilities were substantially reduced when only five repetitions were considered. Right: ROI masks color-coded accorded to detected odorant responses. Glomeruli in which no response was detected are coded gray.

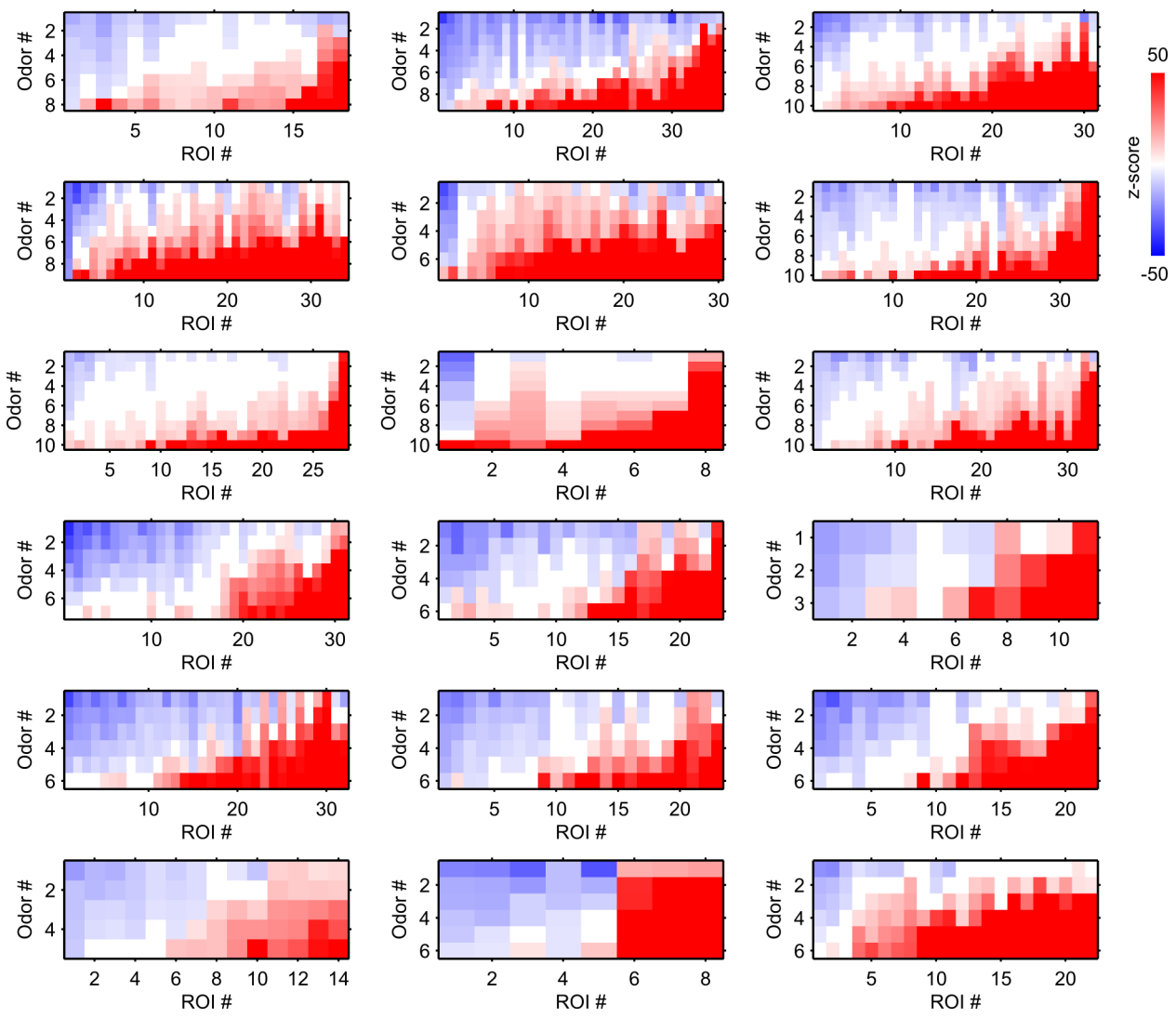

Figure S4 (related to Figure 4). Diversity of response polarity tuning across glomeruli.

Response matrices showing the response of each glomerulus ('ROI') in a field of view to a panel of odorants. Each plot represents one field of view (imaged from 11 mice). Pseudocolor codes the z-score of the peak, low-pass-filtered fluorescence change. Responses were sorted across columns from most excitatory to most suppressive response to enhance visualization of tuning. That is, the same cohort of odorants are represented within each column but in varying order.

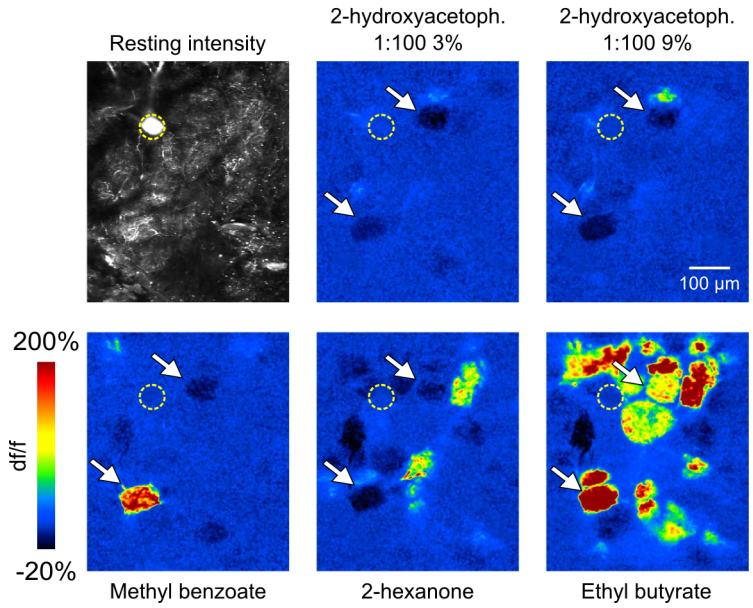

Figure S5 (related to Figure 6). Sparse and selective suppression of glomerular output co-occurs with sparse excitation.

Pseudocolor df/f MT cell odorant response maps imaged from the glomerular layer in a mouse with Channelrhodopsin2-EYFP expressed in M72 OR-expressing olfactory sensory neurons (Smear et al., 2013). Resting fluorescence of the imaged region is shown in upper left. M72 OSN-targeted glomerulus is indicated by yellow circle. Top two maps show response to two concentrations of 2-hydroxyacetophenone (1:100 dilution in liquid, 3 - 9% s.v.), a potent ligand for the M72 OR (Zhang et al., 2012). Responses in the M72 glomerulus are present but masked by YFP fluorescence. Both odorant concentrations drive suppression in two discrete glomeruli(arrows). Suppression is stronger at the higher concentration (9% s.v.). Other odorants also elicit sparse excitation and suppression. Methyl benzoate, another M72 ligand (Zhang et al., 2012), strongly excites one glomerulus suppressed by 2-hydroxyacetophenone and weakly suppresses the other. 2-hexanone (not an M72 ligand) modestly excites several other glomeruli and strongly suppresses others, including the methyl benzoate-excited glomerulus. Ethyl butyrate drives denser excitation with some interspersed suppression, revealing numerous responsive glomeruli in the field of view which were not suppressed by the other odorants.

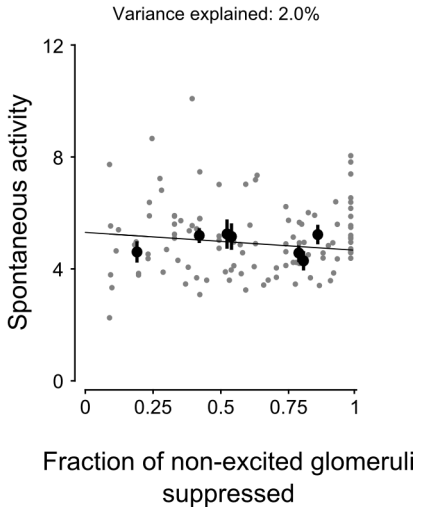

Figure S6 (related to Figure 6). Observations of sparse suppression cannot be explained by varying levels of spontaneous activity.

Spontaneous activity preceding odorant presentation in suppressed glomeruli, plotted as a function of the fraction of non-excited glomeruli in which suppression was detected. Solid line shows linear fit to the binned means ($p>0.1$); error bars indicate SEM. The probability of detecting suppression did not vary with spontaneous activity levels, indicating that when few suppressive responses are detected they are not just detected in the most highly active glomeruli.

Supplemental Information

Includes:

1. Supplemental Figures S1 – S6

Figure S1. Relates to Figure 1 and illustrates that ROIs corresponding to single glomeruli can be identified based on their patterns of spontaneous activity and odorant responses.

Figure S2. Relates to Figure 3 and demonstrates that the time course of activity in individual dendrites innervating the same glomerulus could differ across time, but always responded to odorants with the same polarity.

Figure S3. Relates to Figure 4 and describes a measure of spontaneous activity derived from imaging data that has strong predictive power over the probability of detecting suppressive responses.

Figure S4. Relates to Figure 4 and illustrates that across all experiments, glomeruli showed diversities of tuning for both excitatory and suppressive responses that were glomerulus-specific.

Figure S5. Relates to Figure 6 and shows that glomerular suppression is sparse and glomerulus-specific even when glomerular excitation is sparse in the same field of view.

Figure S6. Relates to Figure 6 and shows that when glomeruli are suppressed, suppression is not preferentially detected in more highly active glomeruli.

2. Supplemental Experimental Procedures

3. Supplemental References

Supplemental Experimental Procedures

Gene-targeted mice

PCdh21-Cre mice were generated by the GENSAT project (Gong et al., 2007) and obtained from the Mutant Mouse Regional Resource Center (Stock #030952-UCD). CCK-IRES-Cre mice and Ai38 (Rosa-GcaMP3) mice were obtained from The Jackson Laboratories (Stock #012706 and #014538, respectively). M72-ChR2 mice were kindly provided by T. Bozza (Northwestern University). All animals were between 2 and 6 months of age by completion of data collection. Mice were housed up to 3/cage and kept on a 12/12 h light/dark cycle. Food and water were available *ad libitum.*

Viral vector expression

Cre-dependent expression of GCaMP3.3 (Tian et al., 2009) or GCaMP6F (Chen et al., 2013) was achieved using the recombinant viral vectors AAV1.hSynap.FlexGCaMP3.3.WPRESV40 or AAV1.hSynap.Flex.GCaMP6f.WPRE.SV40 injected into the anterior piriform cortex (2.34 AP, +1.5 LM, mm relative to bregma at a depth of 3.42 mm relative to brain surface; injection volume 500 nL), or directly into the dorsal OB (injection depth, approximately 300 µm; injection volume 200 – 300 nL). Except as noted below, all mice used for virus injection were homozygous for the allele driving Cre expression. For injection, mice were anesthetized with ketamine (70 mg/kg) and medetomidine (1mg / kg; 'Domitor', Pfizer), placed in a stereotaxic headholder and a circular craniotomy was made over the injection site. Deep brain injections were performed using a 33 gauge metal needle (Hamilton). Virus was injected using a programmable syringe controller (QSI, Stoelting) at a rate of 0.1 µl/min. Injections into the OB were made with a glass pipette. Mice received atipamezole (S.C., Antisedan, 1mg/kg; Pfizer Inc.) at the end of surgery to accelerate recovery from anesthesia. Mice were given carprofen (Rimadyl, 5mg/kg; Pfizer Inc.) as an analgesic immediately prior to surgery, and carprofen-supplemented food (2 mg/tablet) was provided for 4 days post surgery. Mice were single housed after surgery and used 14 - 28 days after virus injection.

Olfactometry

Odorants were presented as dilutions from saturated vapor (s.v.) in cleaned, humidified air using a custom olfactometer under computer control (Bozza et al., 2004; Verhagen et al., 2007). Odorants were presented for 4

seconds. All odorants were obtained at 95 - 99% purity from Sigma-Aldrich and stored under nitrogen. The concentration of the odorants ranged from 0.01% to 2% s.v.. For experiments in awake animals, odorants were diluted in mineral oil so as to yield an estimated final concentration between 1-20 ppm at 1% s.v.. Odorant stimulation trials were separated by 40 seconds to minimize any adaptation by odorant receptors. An odor delivery port was positioned 0.5 - 1.0 cm in front of the animal's nose and a fan at the rear of the animal removed odorants following presentation. In all experiments, stimuli corresponding to different odorants or concentrations were presented in random order. The odorants used included ethyl butyrate, methyl valerate, propanal, butanal, pentanal, 2-methyl pentanal, hexanal, heptanal, benzaldehyde, propyl acetate, butyl acetate, amyl acetate, hexyl acetate, methyl benzoate, methyl salicylate, acetophenone, 2-hydroxyacetophenone, ethyl tiglate, 2-hexanone, isopentylamine, phenethylamine, and n-methyl piperidine. When testing panels of odorants, 8 odorants were selected and included odorant pairs differing by as little as 1 or 2 in carbon chain length while not including more than 3 with the same functional group. In mixture experiments, the concentration of individual odorants was maintained when presented in the mixture by halving the dilution of two-independent odor streams that were then combined in the vapor phase before delivery to the animal.

Imaging

Mice were anesthetized with pentobarbital (50 mg/kg) or isoflurane (0.5 – 2% in O_2) and body temperature was maintained at 37 ºC. A double tracheotomy was performed and artificial inhalation (2 Hz, 200 ms inhalation duration, 150 ml/min peak inhalation flow rate) was used for odorant stimulation independent of breathing (Spors et al., 2006; Wachowiak and Cohen, 2001); isoflurane was delivered directly to the tracheotomy tube, bypassing the nasal cavity.

Animals were secured in a custom head holder for further procedures and imaging, which followed previously established protocols (Bozza et al., 2004; Spors et al., 2006; Wachowiak and Cohen, 2001). A craniotomy covering approximately half of the dorsal surface of the olfactory bulb was performed and covered with 2.5% low-melting point agarose in ringers solution and a glass coverslip. Imaging was carried out with a two-photon microscope coupled to a pulsed Ti:Sapphire laser (Mai Tai HP, Newport or Chameleon HP, Coherent) at 940-980 nm, using a 20X 0.95 N.A. (Olympus) or 16X 0.8 N.A. (Nikon) objective. Estimated average power at the objective front aperture ranged from 50 - 100 mW. In most experiments, scanning and data collection was carried out using a

galvanometer-based system (MOM; Sutter Instruments) under the control of Scanimage 3.9 (Pologruto et al., 2003), with emitted light collected by multialkali photomultiplier tubes (Hamamatsu R6357) and fluorescence movies acquired at 7.5 Hz for imaging of somata and 3.75 Hz for glomerular level imaging. In a few cases (e.g., Figs. 3H, 4A, S2 and S5), higher pixel resolution and higher (15.5 Hz) frame-rate imaging data were collected using a resonance-based scanning system and microscope (Scanbox, Neurolabware) outfitted with GaASP photomultipliers (Hamamatsu H10770B), under the control of Scanbox software.

Head bar and chronic optical window implantation

In a single procedure under general anesthesia induced by ketamine and medetomidine (same doses as above) each animal was implanted with a head-bar for restraint and a chronic window over the OB for optical recordings of neuronal activity. Briefly, after induction of anesthesia, bupivacaine (150 µl of a 1% solution; Sigma-Aldrich, St. Louis, MO) was injected into the epidermis overlying the frontonasal bone for local anesthesia. A midline incision was made and the skull cleaned using 3% H_20_2. The headbar was centered at lambda on the midline and permanently fixed using dental cement. Next, the bone overlying each OB was thinned and a chronic optical window installed (Drew et al., 2010). Mice received atipamezole (same dose as above) at the end of surgery to accelerate recovery from anesthesia. Mice received buprenorphine (01 g/kg) following surgery in addition to the postsurgical treatments described for injections and were allowed to recover for three days before imaging.

Awake imaging

Awake mice were headfixed on a spherical treadmill consisting of a Styrofoam ball floated with air and were allowed to run freely. Before imaging, mice were acclimated for at least 2 sessions (~30 min). Imaging was performed with a 16x 0.8 N.A. objective (Nikon) using the same optical system used in anesthetized experiments. Imaging sessions lasted ~1 hour. In all cases, animals were alert and clearly attended to olfactory stimuli, as evidenced by changes in locomotion and/or sniff frequency. No change in responsivity was observed as a function of locomotion in any cell type.

Data analysis

All data were analyzed using custom scripts written in MATLAB (Mathworks). Pseudocolor glomerular-level activation maps reflect averages of 4-8 trials and were spatially filtered using a Gaussian window with a standard deviation of 1.25 pixels except in Figure 3G,H, Figure 4A, and Supplemental Figure 2. Regions of interest (ROIs) were determined using a semi-automated procedure in which preliminary ROIs were determined manually and later refined to include only pixels whose cross-correlations with the initial ROI were above a user defined threshold (Figure S1). For the experiments in Figures 3F,G a further constraint was imposed that ROIs consist of a single closed polygon.

In all quantitative analyses *df/f* was calculated according to:

$$df/f = \frac{f - f_0}{f_o}$$

where f_0 was taken to be the 2nd percentile of fluorescence values observed within each acquisition (typically 3-6 minutes). Acquisitions in which image brightness was unstable (typically resulting from changes in the meniscus between the window and objective) were discarded. The mean and variance of baseline fluorescence were calculated during a baseline epoch consisting of the 4 second-intervals preceding each odorant presentation. For display of all df/f response maps in the figures, df/f was instead defined relative to this baseline, with f_0 equal to the pre-odor fluorescence, so that negative df/f values represent fractional fluorescence decreases. Fluorescence signals, averaged across trials, were considered to be significantly different from baseline when the peak deviation during the 8 seconds following odorant onset was more than *k* standard deviations from baseline, where k corresponds to a p value of 0.01 using a standard t distribution with the Bonferroni correction and the assumption of 4 independent comparisons per second (k=5.2 for typical trials consisting of 8 odorant presentations). Unfiltered fluorescence time series were used for calculations of latency, power spectra, and in all heatmaps; in all other cases examining the magnitude of response, time series were low-pass filtered using a first order Butterworth filter (to prevent the possibility of ringing) with a cutoff frequency of 0.25 Hz. FFT amplitudes represent the integral of the magnitude of the short-time fast Fourier transform in sliding 4-sec epochs windowed with a Hamming window centered at each time point. For quantification, odorant responses were categorized as suppressive or excitatory based on the direction of the first significant deviation from the baseline epoch fluorescence following odorant exposure. For

visualization, responses were categorized as excitatory if any significant excitatory response was observed (to emphasize suppression preceding delayed excitation).

In mixture experiments, odorant pairs in which at least one odorant elicited an excitatory response were analyzed. The odorant eliciting an excitatory response (or the larger excitatory response if both were excitatory) was considered the 'dominant' odorant. For all comparisons, and for the average time series presented in Figures 7B and 7F, data were normalized to the peak of the dominant odorant response. Trials in which both a significant increase and decrease in fluorescence were observed (biphasic responses) were categorized by the polarity of the first significant deviation from baseline.

Odor correlation in Figure 3 and associated text was calculated as the zero-lag covariance between the time series extracted from each pixel and a binary representation of the stimulus (1 while odor on, zero otherwise). For the purposes of assaying the likelihood of observing suppressive responses, we calculated a spontaneous activity index for each ROI, defined as the average z-scored df/f value during the baseline epoch before odorant stimulation across repeated presentations of a given odorant and normalized to the threshold for detecting a deviation in df/f from the baseline value.

In order to calculate total excitation in Figure 6, all df/f traces were normalized by the standard deviation of odor response amplitudes across all ROIs and odorants tested within a given field of view in order to compensate for experiment-to-experiment variability. Then, total excitation was taken as the sum of the normalized magnitudes of all significant excitatory responses divided by the number of ROIs in each field of view. To determine the 'suppression factor' in Figure 6, we first calculated the difference between the mean df/f value observed in the baseline epoch and the minimum df/f value observed in response to odorant stimulation. This difference was divided by the baseline df/f value to produce a measure meant to approximate the fractional decrease in spike rate. For the analysis in Figures 6G and H, the fraction of suppressive odorants was the number of odorants to which a suppressive response was detected divided by the total number of odorants that did not excite the glomerulus. In both cases, the null distribution was derived from a Monte Carlo simulation in which the real responses to each odorant were randomly assigned to the glomeruli in each field of view. This process was repeated 50,000 times to determine the mean and confidence intervals of the shuffled simulated distribution.

All statistical tests were performed using the Statistics Toolbox in Matlab.

Supplemental References

Bozza, T., McGann, J.P., Mombaerts, P., and Wachowiak, M. (2004). In vivo imaging of neuronal activity by targeted expression of a genetically encoded probe in the mouse. Neuron *42*, 9–21.

Drew, P.J., Shih, A.Y., Driscoll, J.D., Knutsen, P.M., Blinder, P., Davalos, D., Akassoglou, K., Tsai, P.S., and Kleinfeld, D. (2010). Chronic optical access through a polished and reinforced thinned skull. Nat. Methods *7*, 981–984.

Gong, S., Doughty, M., Harbaugh, C.R., Cummins, A., Hatten, M.E., Heintz, N., and Gerfen, C.R. (2007). Targeting Cre recombinase to specific neuron populations with bacterial artificial chromosome constructs. J. Neurosci. *27*, 9817–9823.

Pacifico, R., Dewan, A., Cawley, D., Guo, C., and Bozza, T. (2012). An olfactory subsystem that mediates high-sensitivity detection of volatile amines. Cell Rep *2*, 76–88.

Pologruto, T.A., Sabatini, B.L., and Svoboda, K. (2003). ScanImage: flexible software for operating laser scanning microscopes. Biomed Eng Online *2*, 13.

Saito, H., Chi, Q., Zhuang, H., Matsunami, H., and Mainland, J.D. (2009). Odor coding by a Mammalian receptor repertoire. Sci Signal *2*, ra9.

Smear, M., Resulaj, A., Zhang, J., Bozza, T., and Rinberg, D. (2013). Multiple perceptible signals from a single olfactory glomerulus. Nat Neurosci 16, 1687-1691.

Tian, L., Hires, S.A., Mao, T., Huber, D., Chiappe, M.E., Chalasani, S.H., Petreanu, L., Akerboom, J., McKinney, S.A., Schreiter, E.R., et al. (2009). Imaging neural activity in worms, flies and mice with improved GCaMP calcium indicators. Nat. Methods *6*, 875–881.

Verhagen, J.V., Wesson, D.W., Netoff, T.I., White, J.A., and Wachowiak, M. (2007). Sniffing controls an adaptive filter of sensory input to the olfactory bulb. Nat. Neurosci. *10*, 631–639.

Zhang, J., Huang, G., Dewan, A., Feinstein, P., and Bozza, T. (2012). Uncoupling stimulus specificity and glomerular position in the mouse olfactory system. Mol. and Cell. Neuro. *51*, 79-88.